Relicts in the mist: Two new frog families, genera and species highlight the role of Pantepui as a biodiversity museum throughout the Cenozoic

Antoine Fouquet, Philippe J. R. Kok, Renato Sousa Recoder, Ivan Prates, Agustin Camacho, Sergio Marques-Souza, José Mario Ghellere, Roy W Mcdiarmid, Miguel Trefaut Rodrigues

▶ **To cite this version:**

Antoine Fouquet, Philippe J. R. Kok, Renato Sousa Recoder, Ivan Prates, Agustin Camacho, et al.. Relicts in the mist: Two new frog families, genera and species highlight the role of Pantepui as a biodiversity museum throughout the Cenozoic. Molecular Phylogenetics and Evolution, In press, ⟨10.1016/j.ympev.2023.107971⟩. ⟨hal-04301505⟩

HAL Id: hal-04301505

https://hal.science/hal-04301505v1

Submitted on 23 Nov 2023

HAL is a multi-disciplinary open access archive for the deposit and dissemination of scientific research documents, whether they are published or not. The documents may come from teaching and research institutions in France or abroad, or from public or private research centers.

L'archive ouverte pluridisciplinaire **HAL**, est destinée au dépôt et à la diffusion de documents scientifiques de niveau recherche, publiés ou non, émanant des établissements d'enseignement et de recherche français ou étrangers, des laboratoires publics ou privés.

HAL Authorization

Journal Pre-proofs

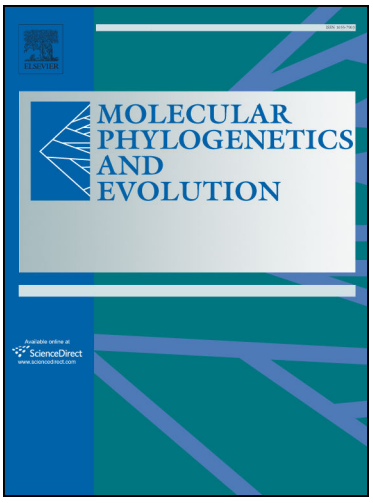

Relicts in the mist: Two new frog families, genera and species highlight the role of Pantepui as a biodiversity museum throughout the Cenozoic

Antoine Fouquet, Philippe J. R. Kok, Renato Sousa Recoder, Ivan Prates, Agustin Camacho, Sergio Marques-Souza, José Mario Ghellere, Roy W. McDiarmid, Miguel Trefaut Rodrigues

PII: S1055-7903(23)00271-3
DOI: https://doi.org/10.1016/j.ympev.2023.107971
Reference: YMPEV 107971

To appear in: *Molecular Phylogenetics and Evolution*

Received Date: 10 February 2023
Revised Date: 21 November 2023
Accepted Date: 21 November 2023

Please cite this article as: Fouquet, A., J. R. Kok, P., Sousa Recoder, R., Prates, I., Camacho, A., Marques-Souza, S., Mario Ghellere, J., McDiarmid, R.W., Trefaut Rodrigues, M., Relicts in the mist: Two new frog families, genera and species highlight the role of Pantepui as a biodiversity museum throughout the Cenozoic, *Molecular Phylogenetics and Evolution* (2023), doi: https://doi.org/10.1016/j.ympev.2023.107971

This is a PDF file of an article that has undergone enhancements after acceptance, such as the addition of a cover page and metadata, and formatting for readability, but it is not yet the definitive version of record. This version will undergo additional copyediting, typesetting and review before it is published in its final form, but we are providing this version to give early visibility of the article. Please note that, during the production process, errors may be discovered which could affect the content, and all legal disclaimers that apply to the journal pertain.

© 2023 Published by Elsevier Inc.

Relicts in the mist: Two new frog families, genera and species highlight the role of Pantepui as a biodiversity museum throughout the Cenozoic

Antoine Fouquet[1*], Philippe J. R. Kok[2,3*], Renato Sousa Recoder[4*], Ivan Prates[5], Agustin Camacho[4], Sergio Marques-Souza[4], José Mario Ghellere[4], Roy W. McDiarmid[6], Miguel Trefaut Rodrigues[4]

[1] *Laboratoire Évolution et Diversité Biologique, UMR 5174, CNRS, IRD, Université Paul Sabatier, Bâtiment 4R1 31062 cedex 9, 118 Route de Narbonne, 31077 Toulouse, France.*

[2] *Department of Ecology and Vertebrate Zoology, Faculty of Biology and Environmental Protection, University of Łódź, 12/16 Banacha Str., Łódź 90-237, Poland.*

[3] *Life Sciences, The Natural History Museum, Cromwell Road, London SW7 5BD, United Kingdom.*

[4] *Universidade de São Paulo, Instituto de Biociências, Departamento de Zoologia, São Paulo, SP, Brazil.*

[5] *Department of Ecology and Evolutionary Biology and Museum of Zoology, University of Michigan, Ann Arbor, MI, USA.*

[6] *Department of Vertebrate Zoology, National Museum of Natural History, Smithsonian Institution, PO Box 37012, Washington, DC 20013, USA*

* Co-first authors and co-corresponding authors: e-mails: fouquet.antoine@gmail.com; pjrkok@gmail.com; renatorecoder@gmail.com

1. We discovered two new frog species from the Neblina massif, Pantepui
2. Both species represent deeply rooted new lineages within Brachycephaloidea
3. Morphological data also support the creation of two new family and genus-level taxa
4. These results confirm the role of "museum" played by Pantepui during Cenozoic

Authors contribution statement

R.S.R, I.P., A.C., S.M.-S., J.M.G., R.W.McD., M.T.R. undertook field work led by M.T.R.

A.F. produced the molecular data and analyses and the main writing.

A.F. produced the segmentation and volume renderings. P.J.R.K. led the osteological analyses. R.S.R examined the external morphology and myological examination.

M.T.R supervised the findings of this work. All authors discussed the results and contributed to the final manuscript

Abstract. The iconic mountains of the Pantepui biogeographical region host many early-diverging endemic animal and plant lineages, concurring with Conan Doyle's novel about an ancient "Lost World". While this is the case of several frog lineages, others appear to have more recent origins, adding to the controversy around the diversification processes in this region. Due to its remoteness, Pantepui is challenging for biological surveys, and only a glimpse of its biodiversity has been described, which hampers comprehensive evolutionary studies in many groups. During a recent expedition to the Neblina massif on the Brazil-Venezuela border, we sampled two new frog species that could not be assigned to any known genus. Here, we perform phylogenetic analyses of mitogenomic and nuclear loci to infer the evolutionary relationships of the new taxa and support their description. We find that both species represent single lineages deeply nested within Brachycephaloidea, a major Neotropical clade of direct-developing frogs. Both species diverged >45 Ma from their closest relatives: the first is sister to all other Brachycephaloidea except for *Ceuthomantis*, another Pantepui endemic, and the second is sister to Brachycephalidae, endemic to the Brazilian Atlantic Forest. In addition to these considerable phylogenetic and biogeographic divergences, external morphology and osteological features support the proposition of two new family and genus-level taxa to accommodate these new branches of the amphibian tree of life. These findings add to other recently described ancient vertebrate lineages from the Neblina massif, providing a bewildering reminder that our perception of the Pantepui's biodiversity remains vastly incomplete. It also provides insights into how these mountains acted as "museums" during the diversification of Brachycephaloidea and of Neotropical biotas more broadly, in line with the influential "Plateau theory". Finally, these discoveries point at the yet unknown branches of the tree of life that may go extinct, due to global climate change and zoonotic diseases, before we even learn about their existence, amphibians living at higher elevations being particularly at risk.

Keywords. Amazonia, Biogeography, Guiana Shield, Neotropics, Phylogeny, Taxonomy

Journal Pre-proofs

1. Introduction

The Neotropical realm hosts the most diverse terrestrial ecosystems on the planet (Jenkins et al., 2013). The role of the formation of the Andean Cordillera and associated landscape modifications throughout the continent have become paradigmatic for explaining the origins of Neotropical biodiversity (Gentry, 1982; Hughes and Eastwood, 2006; Hoorn et al., 2010; Esquerre et al., 2019). These mountains acted both as cradles (promoting *in situ* speciation) and museums (serving as refugia to isolated relict species from groups that went extinct elsewhere), thereby leading to neo- and paleo-endemisms, respectively (Rangel et al., 2018; Rahbek et al., 2019; Azevedo et al., 2020; Boschman and Condamine, 2022). The Andean uplift progressed northward during the Paleogene and intensified during the Neogene around 12–4.5 Ma (Garzione et al., 2008; Hoorn et al., 2010; Chen et al., 2019), affecting regional climate and hydrology and resulting in the modern configuration of the Amazon drainage some 10 Ma (Hoorn et al., 2010, 2017).

These landscape changes have affected the diversification of many animal and plant lineages, notably of amphibians. This is the case of the families Centrolenidae (Castroviejo et al., 2014) and Dendrobatidae (Santos et al., 2009), two frog clades that have primarily diversified in the Andes, often following its northward orogeny, and subsequently feeding the adjacent lowlands with lineages. Moreover, no fewer than nine different genera of Brachycephaloidea (*Bryophryne, Lynchius, Microkayla, Niceforonia, Phrynopus, Psychrophrynella, Qosqonophryne, Tachiramantis, Serranobatrachus*) are endemic to the Andean chain or only marginally distributed outside of it. These and other amphibian clades have emerged as particularly suitable models to investigate the role of mountains and landscape modifications in continental-level diversification because of their relatively low dispersal abilities, high endemism, and conserved and narrow ecological breadths (e.g., Giam et al., 2013; Rolland et al., 2018).

In contrast with the Andes and Amazonian lowlands, the role of the Pantepui region in Neotropical diversification has been much less emphasized. This much older highland formation consists of peculiar high-elevation sandstone table mountains surrounded by upland forests and savannas (Kok, 2013; Rull and Vegas-Vilarrúbia, 2020). Since the first explorations of the Guiana Shield highlands and the famous novel “The Lost World” by Sir Arthur Conan Doyle (1912), these “islands in the sky” have been thought to harbor isolated relict lineages (Rull, 2004). In contrast with the predominantly sedimentary and dynamic Andes, the cratonic Guiana Shield has remained relatively stable geologically throughout the Cenozoic (Hoorn et al., 2010). Moreover, since South America has drifted little latitudinally over the past 100 My, its northern part has remained predominantly tropical (Hammond, 2005). The craton itself was covered by sedimentary layers 1,600 to 1,000 Ma, and epeirogenic uplifts during the late Mesozoic, followed by intense erosion by wind and weathering, gradually led to the present-day geomorphology of Pantepui (Huber, 2005). Like the Andes, this region hosts many ancient (near-*) endemic lineages of amphibians: *Stefania*, Oreophrynella, Minyobates, Nesorohyla, Myersiohyla, Tepuihyla*,* and *Ceuthomantis* (Heinicke et al., 2009; Santos et al., 2009; Kok, 2013; Kok et al., 2017, 2018; Pinheiro et al., 2019; Ortiz et al., 2022). There are also many endemic lizard genera such as *Adercosaurus, Kaieteurosaurus, Pantepuisaurus*, *Riolama, Yanomamia* (Myers and Donnelly, 2001; Kok, 2005; 2009; 2015; Pellegrino et al., 2018; Recoder et al., 2020), a recently described endemic snake genus (Kok and Means, 2023) as well as endemic birds (sometimes early-diverging, e.g., Mayr and Phelps, 1967), mammals (e.g., Leite et al., 2015), invertebrates (e.g., Kok et al., 2019), and plants (e.g., Steyermark, 1986; Berry and Riina, 2005). Most of the endemic anuran genera have diverged before the Neogene from relatives

that have themselves, in most cases, diversified throughout the Neotropics both in the lowlands and in the highlands (e.g., Heinicke et al., 2018; Kok et al., 2017, 2018). A few enigmatic anuran taxa such as *Metaphryniscus* and *Dischidodactylus* have not yet been included in molecular phylogenetic studies, but given their morphological singularities, possibly correspond to ancient lineages as well.

The occurrence of such ancient and isolated lineages concurs with the "Plateau theory" (Mayr and Phelps, 1967), originally formulated for birds by Tate (1930, 1938) and also coined as the "Lost World hypothesis" (Rull, 2004; see Kok, 2013 for a comprehensive summary). This hypothesis states that extant tepui summit species are derived from highland ancestors that occupied a large continuous plateau that was gradually eroded and dissected into several isolated tepuis during the Paleogene (Kok, 2013). However, the existence of shallow divergences across many neighboring tepui summit species also suggests recent dispersals and interconnectivity, possibly during the cold climatic cycles of the Pleistocene (Kok et al., 2012; Salerno et al., 2012; Kok, 2013). The considerable vertical displacement of ecosystems during the Pleistocene and Holocene glaciation cycles, suggested by paleoclimatic and palynological data, makes the persistence of demographically large and biodiverse communities on the summits unlikely (Rull, 2004), although some highland populations have probably remained isolated and adapted to changing conditions, while others followed particular habitats as conditions shifted altitudinally (Kok, 2013). Additionally, upland (i.e., lower elevations than the summits) lineages originating in Pantepui also diversified further in the lowlands during the Neogene (e.g., *Adelastes, Anomaloglossus, Otophryne, Adelophryne*) (Fouquet et al., 2012, 2021; Vacher et al., in press). Therefore, the most recent speciation events most likely resulted from dispersals (either active or passive, see Kok, 2013; Kok et al., 2017), while the persistence of so many ancient endemic lineages throughout the Cenozoic has probably been facilitated by the relative geological long-term stability and the existence of marked elevational gradients allowing range displacements and persistence during fluctuating climatic conditions (e.g., Wiens et al., 2019).

Despite this emerging picture, our understanding of tepui summits' biodiversity and evolution remains fragmentary, a situation in part due to the difficult access and long-lasting political turmoil in the region. As far as amphibians are concerned, recent efforts and tissue collections for molecular analyses have mainly focused on tepuis located east of the Rio Caroní in eastern Venezuela and Guyana (e.g., MacCulloch and Lathrop, 2002; 2005; MacCulloch et al., 2008; Kok, 2023a,b; Kok et al., 2012; 2015; 2017; 2018), while the western and the southern parts of Pantepui are nowadays much less explored. However, the western parts of Pantepui, including Serra da Neblina (or Cerro de la Neblina) have been extensively surveyed in the 1980s on the Venezuelan side, with no fewer than 144 scientists involved in 10 field expeditions covering 14 different camps in that specific area (Brewer-Carías, 1988). Herpetologists such as R.B. Cocroft, C.J. Cole, L. Ford, R.W. McDiarmid, C. Myers, A. Paolillo and R.G. Zweifel extensively collected in the area, which resulted in several reports, species lists (e.g., Brewer-Carías, 1988), and new taxon descriptions (e.g., Zweifel, 1986; Myers et al., 1993; see McDiarmid and Donnelly, 2005 for a comprehensive overview). Nevertheless, a substantial number of the new species reported in these studies remains undescribed (McDiarmid and Donnelly, 2005).

During a recent scientific expedition supported by the Brazilian Army and local Yanomami communities, members of our team surveyed the highest part of the Brazilian portion of this tepui complex. This new effort resulted in the collection of specimens and tissue samples from two species of frogs that could not be assigned to any known genus, yet seemingly belonging to Brachycephaloidea, a major lineage (ca. 1,200 species) of Hyloidea

that contains some of the most species-rich genera among vertebrates (Padial et al., 2014; Heinicke et al., 2009, 2015, 2018; Barrientos et al., 2020; Motta et al., 2021). Evolutionary relationships remain ambiguous within Brachycephaloidea, hampering our understanding of the diversification processes of this clade (ibid). Remarkably, previous phylogenomic studies (Feng et al., 2017; Heinicke et al., 2018; Hime et al., 2021) suggest that the first diverging extant lineage within Brachycephaloidea is *Ceuthomantis*, one of the oldest (ca. 60 Ma) Pantepui endemic genera, suggesting that this region might have been key to the diversification of the world's most diverse amphibian radiation.

Here, we investigate the phylogenetic relationships and the timing of diversification of these two enigmatic frog species within the Brachycephaloidea radiation. Based on our findings, we discuss the implications of these newly discovered lineages for the origin of Brachycephaloidea, the Pantepui biota, and Neotropical faunas in general. We also formally name and describe the two new, and yet seemingly ancient, frog species, which requires the erection of two new genera and families.

2. Materials and Methods

2.1. Study area and field work

Serra da Neblina is a highly eroded sandstone plateau, part of the Roraima Formation, located on the Brazilian-Venezuelan border and overlaying the Precambrian basement. Its highest mountain, Pico da Neblina, is the highest point of Brazil (2,995 m) and South America excluding the Andes. Covering an area approximately 50 km long and 20 km wide, mostly in Venezuelan territory, the massif is one of the largest of the Pantepui region. It is entirely surrounded by lowlands and uplands covered by Amazonian forest, which reach about 1,000 m, being then gradually replaced by montane forest with trees of variable height up to an elevation of 1,800 m. Above this elevation, montane forests progressively give space (on the plateaus and highest peaks) to scrublands with scattered trees and meadows on peat and extensive bogs. Fields of large bromeliads cover extensive areas of the plateaus. Except for disturbance from predominantly near-artisanal mining, the region has generally remained well-preserved under the protection of Parque Nacional do Pico da Neblina in Brazil and Parque Nacional de la Serrania de Neblina in Venezuela which broadly overlap with the Yanomami territory (Fig. 1).

Our camp was settled by the Brazilian Army at Bacia do Gelo (geographic coordinates: 0.79286 N, 66.02495 W), an extensive plateau at 2,000 m elevation facing the Pico (peak) da Neblina on the northern border of the Brazilian state of Amazonas. Our campsite was close to a 2 m wide stream with dark tinted waters. The area is prone to flooding, as the frequent heavy rains often lead to the sudden formation of waterfalls along the cliffs of the peak, which drain into the stream and make it overflow within minutes onto the adjacent swamps and bogs. The local vegetation is dominated by low to mid-size shrubs and meadows where Bromeliaceae (especially *Brocchinia tatei*), Rapateaceae, and Theaceae are abundant in a mostly wet peat, with ferns covering the stream's banks (Fig. 1, Supplementary Fig. S1–S2). Slightly higher areas near the slopes of those isolated peaks, as well as stream banks, are covered by denser and taller vegetation (up to 5 m), where palms (*Euterpe* sp.) are abundant.

Besides collecting at Bacia do Gelo, we also sampled the slopes and the summit of the Pico da Neblina. The path to the peak led us across rocky and steep hillslopes where the above-cited waterfalls ran a few days earlier. The vegetation on these slopes was mostly low and sparse, composed of grasses, abundant thickets of *Heliamphora* pitcher plants, and small bushes. Closer to the mountaintop, the ground was formed by loose gravel and rocks, sand, and peat bog (Supplementary Fig. S1–S2). We undertook fieldwork from 15–23 November 2017. Additional data on habitat and field sampling are provided in Recoder et al. (2020).

Hand-captured specimens were euthanized with an intraperitoneal injection of lidocaine hydrochloride. We then obtained tissue samples (pieces of liver or muscle preserved in 95% ethanol) from all individuals. These tissue samples were later deposited under their original field numbers (MTR series) in the tissue collection of the Department of Zoology, Instituto de Biociências, Universidade de São Paulo, Brazil. Following tissue sampling, specimens were fixed in 10% formalin and then transferred to 70% ethanol for permanent storage. Voucher specimens were deposited in the Herpetological Collection of Museu de Zoologia, Universidade de São Paulo (MZUSP), keeping their original field tags for future reference.

2.2. Evolutionary inference

2.2.1. Generation of molecular data

To infer the phylogenetic placement of the newly sampled frogs (and thus inform their taxonomic assignment), we selected 45 terminals representative of major lineages of Hyloidea, spanning all families except for Rhinodermatidae. Preliminary analyses indicated that the new species are likely nested within Brachycephaloidea. We built a genus-level matrix limiting missing data as much as possible and including most Brachycephaloidea genera (18) except for *Atopophrynus*, *Geobatrachus* and *Dischidodactylus*, for which no molecular data or genetic material are available, and for *Serranobatrachus*, which was recently described (Arroyo et al., 2022). We also did not include three genera of Pristimantinae (*Yunganastes*, *Lynchius*, *Tachiramantis*) and five genera of Holoadeninae (*Bahius, Euparkerella, Microkayla, Psychrophrynella, Qosqophryne*) with scarce molecular data available but previously found to be nested within clades represented in our dataset. There is strong evidence for the monophyly of the genera included in our analyses (notably the species-richest genera *Pristimantis*, *Eleutherodactylus*, *Craugastor*; Padial et al. 2014; Mendoza et al. 2015; Hutter et al. 2017; Motta et al. 2021) and only genera nested within well-defined clades were not included (except those missing genetic data). All deep branches of Brachycephloidea are represented, thus limiting the impact of the incomplete taxonomic sampling where focal species are nested. The main reason for this approach is to improve the robustness of topological and temporal inferences (e.g., Sanderson and Shaffer 2002; Roure et al. 2013; Smith et al. 2020) given the old ages of the relationships involved. Outgroups included *Calyptocephallela* and two representatives of Microhylidae (*Gastrophryne* and *Microhyla*), totaling 50 terminals.

We obtained whole (or nearly complete) mitogenomic data for all terminals (37 from GenBank, 13 newly generated). Newly generated data were obtained via shotgun sequencing (GenBank accession numbers [to be added upon manuscript acceptance] and detailed sample information are provided in Supplementary Table S1). We used 200 ng of genomic DNA for genomic library construction. Libraries were prepared using the Illumina TruSeq Nano DNA

Sample Prep kit following supplier instructions at the Genotoul-Get-PlaGe core facility (Toulouse, France). Briefly, genomic DNA was fragmented by sonication, and fragments were then size-selected (50–400 bp), adenylated, and ligated to indexed sequencing adapters. Eight cycles of Polymerase Chain Reaction (PCR) were applied to amplify libraries before quantification and validation. Libraries were multiplexed and sequenced on one lane of an Illumina NovaSeq 6000 flow cell (Illumina Inc., San Diego, CA). Read assembly was performed using NOVOPlasty 4.3 (Dierckxsens et al., 2017), a seed-extend based assembler optimized for circular plastid genomes, to perform a circularized assembly, with default parameters and different seeds depending on the taxa and the success of the assembly. Annotations were transferred to the new mitogenomes from the mitogenome of *Leptodactylus fallax* (NC_056366) after alignment. The control region, the third position of each codon, and tRNA genes were not included in the phylogenetic analyses to minimize the effects of substitution saturation. Sequences of the 12S and 16S ribosomal genes were realigned on the MAFFT online server (Katoh et al., 2017) under the E-INS-i option, considering the reading frame option for each CoDing Sequence (CDS).

We further complemented this mitogenomic dataset with six nuclear (nuDNA) loci (POMC: 558 base pairs [bp], RAG1: 1374 bp, TYR: 675 bp, NCX1: 1278 bp, CXCR4: 630 bp, SLC8A3: 1,092 bp; totaling 5,607 bp) obtained via Sanger sequencing following standard protocols and complemented with sequences available in GenBank (details of primers are available in Supplementary Table S2). In order to reduce the impact of missing data, these nuDNA data were at least congeneric with the mitogenomic data (i.e., not always conspecific), depending on sequence availability. We carefully verified, using literature and additional analyses, that the species used across loci formed monophyletic groups and that no erroneous sequences (misidentified in GenBank) were used. The nuclear matrix was complete except for five terminals without SLC8A3 sequences and up to two loci for five of the terminals. In total, 43 of the 50 terminals included had complete nuclear datasets.

2.2.2. Phylogenetic analyses and divergence time estimation

Our final DNA alignment consisted of 16,033 bp, comprising 10,471 bp of mtDNA (12S–16S: 2,975; 3,748 for the mtDNA CDS) and 5,562 bp of concatenated nuDNA. We predefined six partitions: one for the rRNA genes (12S and 16S), one for each codon position of the concatenated mtDNA CDS regions (n=2), and one for each nuDNA CDS region (n=3). We selected the best-fit model of evolution for each partition using ModelFinder in IQTREE (Chernomor et al., 2016; Kalyaanamoorthy et al., 2017) according to the Bayesian Information Criterion (BIC). We inferred time-calibrated phylogenetic trees in BEAST 2.5.2 (Bouckaert et al., 2014) using a birth-death tree prior for mt and nuDNA concatenated, which were also analyzed separately. We used unlinked substitution models following results from the ModelFinder analysis and unlinked clock models. Trees were linked. Divergence time estimation was implemented using an uncorrelated relaxed lognormal clock model for the distribution of rates among branches for each partition (Drummond et al., 2006). We relied on secondary calibrations based on Hime et al. (2021), which incorporated an extensive nuclear genomic dataset (220 loci, 291 kb) including all major frog lineages. Specifically, we assumed a normal prior distribution for eight nodes, as follows: (1) the Most Recent Common Ancestor (MRCA) of Neobatrachia (excluding *Heleophryne*) (mean = 134.3; 95% Highest Posterior Density [HDP] intervals = 128.0–140.6), which corresponds to the root of the tree; (2) the MRCA of Hyloidea+Calyptocephallelidae (123.3; 116.3–130.2); (3) the MRCA of Hyloidea excluding Rhinodermatidae (66.8; 62.7–71.1); (4) the MRCA of Hyloidea excluding

Rhinodermatidae and Neoaustrarana (65.0; 60.9–69.1); (5) the MRCA of Bufonidae (48.2; 44.1–52.4); (6) the MRCA of Hylidae *sensu lato* (Arborana) (58.8; 55.0–62.8); (7) the MRCA of Dendrobatoidea (38.1; 33.9–42.3); (8) the MRCA of Brachycephaloidea (54.4; 50.4–58.5) without including our new species. Monophyly was constrained for (2), (3), (4) and (6).

We set two independent Markov chain Monte Carlo (MCMC) runs of 100 million iterations each, recording every 1,000 iterations and discarding the first 10% of iterations as burn-in. We combined the resulting log files and the posterior samples of trees from the two runs using LogCombiner 2.5 (Bouckaert et al., 2014). We ensured convergence and proper chain mixing by inspecting time-series plots of model parameters based on the combined log files. Mixing was considered adequate when parameters achieved an effective sample size above 200 (obtained for all parameters). We then extracted a maximum clade credibility tree (based on 10% of the trees, randomly selected using LogCombiner, thus 18,002 resulting trees) using Tree Annotator 2.5 (Bouckaert et al., 2014).

2.3. Morphology

2.3.1. External morphology

We examined the external morphology of 33 specimens of "Species 1" (*Neblinaphryne mayeri* gen. nov. sp. nov.; see below) and 22 specimens of "Species 2" (*Caligophryne doylei* gen. nov. sp. nov.). We mainly followed Lynch and Duellman (1997) and Duellman and Lehr (2009) for diagnoses and descriptions, with modifications. Sex was determined by the presence of vocal slits or sacs and direct inspection of gonads via a lateral abdominal incision. We took the following measurements with digital calipers to the nearest 0.01 mm: SVL, snout–vent length; HL, head length (from the posterior margin of lower jaw to tip of snout); HW, head width (measured at the level of the rictus); IND, internarial distance; END, eye to nostril distance; ED, eye diameter (measured horizontally); IOD, interorbital distance; UEW, upper eyelid width; TD, tympanum diameter (measured horizontally); ARM, arm length (from the posterior margin of the thenar tubercle to the elbow); HAN, hand length (from the posterior margin of the thenar tubercle to the tip of the third finger); TH, thigh length (from vent to knee); TL, tibia length; TAL, tarsal length; FTL, foot length (from the proximal border of the inner metatarsal tubercle to the tip of the fourth toe). We rounded all raw measurements to one decimal to avoid pseudo-precision. The relative length of fingers I and II was determined by adpressing them against each other; lengths of toes III and V were compared when both were adpressed against Toe IV.

2.3.2. Osteology

Three specimens of each of the new species were µCT-scanned (kV = 40–70, resolution < 20 µm) using a Bruker Skyscan 1176 at the Universidade de São Paulo, Brazil. Segmentation of the full skeleton of one paratype specimen of each species (*Neblinaphryne mayeri* gen. nov. sp. nov. MZUSP A159552/MTR 40321; *Caligophryne doylei* gen. nov. sp. nov. MZUSP A159536/MTR 40248) was performed using Avizo (FEI Visualization Sciences Group, Burlington, MA, USA) and Biomedisa (Lösel et al., 2000), while additional paratype specimens (*Neblinaphryne mayeri* gen. nov. sp. nov. MZUSP A159555/MTR 40329; MZUSP A159580/MTR 40362; *Caligophryne doylei* gen. nov. sp. nov. MZUSP A159548/MTR

40341; MZUSP A159530/MTR 40230) were examined using volume renderings. µCT-scans and surface renderings will be deposited at MorphoSource (www.morphosource.org) upon manuscript acceptance. We described osteological features of the two new species and compared 14 remarkable features to those of 25 specimens representing 21 genera and all subfamilies of Brachycephaloidea (from resources available in MorphoSource), notably including *Ceuthomantis* and *Dischidodactylus*, the two other genera from the Pantepui region in this clade (character states in Supplementary Table S3). These features are: (1) condition of the skull (massive vs. moderate); (2) condition of the sphenethmoid complex (free; contacting; or fused with nasals); (3) state of the septomaxillae (present or absent/vestigial); (4) state of the nasals (medially fused or not); (5) condition of the frontoparietal (exostosed or not; crested or not); (6) condition of the lateral arms of the parasphenoid (free; contacting; or fused with the medial ramus of the pterygoid); (7) condition of the vomers relative to the sphenethmoid (free; contacting; or fused); (8) condition of the vomers relative to the neopalatine (free; contacting; or fused); (9) presence/absence of vomerine teeth; (10) condition of the maxilla relative to the squamosal (directed towards/fused with the zygomatic ramus of the squamosal or not); (11) condition of the maxilla relative to the quadratojugal (free; contacting; or fused); (12) presence/absence of a columella; (13) number of vertebrae in the vertebral column; (14) presence/absence of a vertebral shield. Osteological terminology followed Trueb (1973).

2.3.3. Musculature

We examined myological characters related to the insertion of the *m. iliacus externus* and the *m. tensor fasciae latae*, two muscles originating on the iliac shaft. These muscles present extensive variation in frogs (Dunlap, 1960) and certain states have been suggested to represent synapomorphies for some clades of Brachycephaloidea (Ospina-Sarria and Grant, 2021). For this purpose, we made a lateral incision on the skin of MTR40357 (*Neblinaphryne mayeri* gen. nov. sp. nov.) and MTR40260 (*Caligophryne doylei* gen. nov. sp. nov.) to expose the superficial pelvic and thigh muscles. The attachment of the muscles was observed under a stereomicroscope. Terminology follows Dunlap (1960) and Ospina-Sarria and Grant (2021).

3. Results

3.1. Time calibrated phylogenetic reconstructions

Phylogenetic analyses based on the mitogenomic and nuDNA data combined recovered the two new species as nested within Brachycephaloidea (Fig. 2). Both species were inferred to have diverged at least 45 Ma from their respective closest relatives. *Neblinaphryne mayeri* gen. nov. sp. nov. was found to be sister to all Brachycephaloidea except for *Ceuthomantis* (posterior probability [pp] = 1.0). *Caligophryne doylei* gen. nov. sp. nov. was recovered as sister to Brachycephalidae (pp = 1.0). Other relationships within Brachycephaloidea were all highly supported, with the exception of two nodes within Strabomantidae (Fig. 2). This topology notably supports a clade formed by Brachycephalidae + *Caligophryne doylei* gen. nov. sp. nov. and Eleutherodactylidae. In turn, this clade is sister to a clade formed by Strabomantidae + Craugastoridae. The unconstrained relationships among Hyloidea lineages are also strongly supported with a single exception within Neoaustrorana.

When analyzed separately, nuDNA data similarly support *Neblinaphryne mayeri* gen. nov. sp. nov. as the sister lineage of all Brachycephaloidea except *Ceuthomantis*, diverging ca. 55 Ma with strong support (pp = 1.0) (Supplementary Fig. S3). In contrast, mitogenomic data alone support this new species as the sister lineage of *Ceuthomantis*, diverging ca. 53 Ma with strong support (pp = 0.96) (Supplementary Fig. S3). Both the nuclear and mitochondrial datasets support the position of *Caligophryne doylei* gen. nov. sp. nov. as the sister lineage of Brachycephalidae, diverging ca. 47 Ma with strong and moderate support, respectively (pp = 1.0; 0.94).

Within Brachycephaloidea, nuDNA data inferred an early divergence of Brachycephalidae + *Caligophryne doylei* gen. nov. sp. nov. relative to other families (Supplementary Fig. S3), followed by the divergence of Eleutherodactylidae. The latter is sister to a clade formed by Craugastoridae and Strabomantidae with strong support (pp = 1.0). However, mitogenomic data alone support a clade formed by Brachycephalidae, Eleutherodactylidae and Craugastoridae as the sister group of Strabomantidae with strong support (pp = 1.0). The position of Craugastoridae is also notably incongruent between mtDNA and nuDNA, although poorly supported with nuDNA.

3.2. Morphology and supra-specific taxonomic implications

Full morphological descriptions are provided in the taxonomic accounts below. Here, we highlight the most striking features supporting our taxonomic decisions above the species level.

Heinicke et al. (2009) suggested that all Brachycephaloidea have arciferal pectoral girdles (pseudofirmisternal in a few taxa) and partially fused calcanea and astragali while lacking intercalary elements in the digits. Ospina-Sarria and Grant (2021) suggested that in all Brachycephaloidea the *m. iliacus externus* originates via a single head from the iliac shaft. We confirm these character states in both of our new species (Supplementary Fig. S5), which, however, differ from other Brachycephaloidea in several ways. *Neblinaphryne mayeri* gen. nov. sp. nov. is a small-bodied (14.0–19.2 mm in males) semi-fossorial species with very few remarkable external characters except the mucronate tips of fingers and toes (Fig. 3; Supplementary Fig. S4). Osteologically, however, the absence/highly vestigial state of the septomaxillae (see Figs 4–5; Supplementary Fig. S6), and pointed terminal phalanges, seem unique among Brachycephaloidea. *Caligophryne doylei* gen. nov. sp. nov. is a medium-sized (19.7–29.6 mm in males) terrestrial frog with striking blue iris, massive head, and concealed parts of legs black with small white flecks as well as dorsolateral black blotches (probably to elicit predator confusion) (Fig. 6). This species also stands out among most other anurans by osteological features, notably a massive, hyperossified skull with exostosed frontoparietal and parietal crests (a character also shared with several species of *Stefania* and *Strabomantis*) (Figs 7–8; Supplementary Fig. S6). Although having unclear implications for the phylogenetic affinities and diagnosis of *Caligophryne doylei* gen. nov. sp. nov., we note the presence of extensive paired calcified processes (possibly calcified endolymphatic sacs; Dempster, 1930) extending through the intervertebral foramina and under the transverse processes of vertebrae, shielding the ventral surface of the vertebral column (to some extent also present in some species of the Pantepui endemic genus *Stefania*, e.g., Kok, 2023a).

Our analyses (molecular and morphological) recovered the two new species to be highly divergent from any other known frog species. The position of *Neblinaphryne mayeri*

gen. nov. sp. nov. is conflictual between nuDNA and mtDNA, both being strongly supported. It has been reported that mtDNA is inherently prone to substitution saturation and long-branch attraction, even when the third codon positions are removed, especially for relationships older than 50 Ma (Fouquet et al., 2022), which is the case of *Neblinaphryne mayeri* gen. nov. sp. nov. Therefore, we may expect the relationships inferred from nuDNA to be more reliable in this case. The phylogenetic position of *Neblinaphryne mayeri* gen. nov. sp. nov. according to nuDNA implies that it cannot be assigned to any known frog genus or family, a hypothesis also supported by morphological features (external and osteological). As far as *Caligophryne doylei* gen. nov. sp. nov. is concerned, it could potentially be assigned to Brachycephalidae since both are sister lineages. Nevertheless, it should be noted that Brachycephalidae is restricted to the Atlantic Forest of coastal Brazil, and that the morphology of *Caligophryne doylei* gen. nov. sp. nov., notably its peculiar osteology relative to that of *Brachycephalus* and *Ischnocnema*, is so distinctive that we consider the erection of a separate family to allocate this highly divergent Pantepui lineage justified. Finally, divergence times estimated between these new species and their closest relatives are as old (>45 Ma) as most other pairs of anuran families (Hime et al., 2021). Therefore, we propose two new genera and families to accommodate the two new species.

3.3. Taxonomy

Class Amphibia Linnaeus, 1758

Order Anura Duméril, 1805

Superfamily Brachycephaloidea Günther, 1858

Neblinaphrynidae fam. nov.

Type genus: *Neblinaphryne* Fouquet, Kok, Recoder, Prates, Camacho, Marques-Souza, Ghellere, McDiarmid, Rodrigues, 2023.

Diagnosis. The new family is distinguished from all other families within Hyloidea on the basis of molecular characters (see Fig. 2). It is considered a member of Brachycephaloidea based on molecular characters and the presence of arciferal pectoral girdles, partially fused calcanea and astragali, while lacking intercalary elements in the digits (Figs 4–5; Supplementary Fig. S6), and *m. iliacus externus* originating via a single head from the iliac shaft (Supplementary Fig. S5). The only unique phenotypic character states distinguishing this family seem to be the absence/highly vestigial state of septomaxillae, and the pointed terminal phalanges (Figs 4–5; Supplementary Fig. S6; Table S3). Other characteristics are unique in combination: (1) frontoparietal smooth, cranial crests absent; (2) dentigerous process of vomer absent, vomers free of contact with any other bone; (3) Finger III with mucronate tip; (4) Toes II–IV with mucronate tips (Fig. 3); (5) *m. iliacus externus* originating anteriorly and extending in parallel alongside the entire length of the iliac shaft; (6) *m. tensor fasciae latae* originating anteriorly on the iliac shaft, immediately posterior to the sacral diapophyses (Supplementary Fig. S5).

Comparison with other families All the other Brachycephaloidea have well-developed septomaxillae and T-shaped terminal phalanges.

Content. One genus, *Neblinaphryne* gen. nov.

Distribution. Known only from the Neblina massif, Pantepui, northeastern South America

***Neblinaphryne* gen. nov.**

Type species: *Neblinaphryne mayeri* Fouquet, Kok, Recoder, Prates, Camacho, Marques-Souza, Ghellere, McDiarmid, Rodrigues, 2023

Diagnosis. Neblinaphrynidae being monotypic, the diagnosis of the genus is the same as for the family.

Content. One species**,** *Neblinaphryne mayeri* sp. nov.

Distribution. Known only from the Neblina massif, Pantepui, northeastern South America

Etymology. The generic name refers to the Pico de Neblina massif and is a combination of "neblina" meaning "fog" in Portuguese and Spanish, and "*phryne*", meaning "toad" in Ancient Greek.

***Neblinaphryne mayeri* sp. nov.**

Holotype. MZUSP A159564 (field number MTR 40344; Fig. 3), an adult female from the trail to Pico da Neblina summit, in the highlands of the Serra da Neblina (Fig. 1), Parque Nacional do Pico da Neblina, Santa Isabel do Rio Negro, Amazonas State, Brazil (0.79917 N, 66.01028 W; 2,600 m above sea level [a.s.l]; map datum WGS84); collected on 21 November 2017 by M. T. Rodrigues, A. Camacho, F. Dal Vechio, I. Prates, J. M. Ghellere, R. Recoder and S. Marques-Souza.

Paratypes (n = 32) (Supplementary Fig. S4). MZUSP A159565–A159572, MZUSP A159577–A159584 (field numbers MTR 40345, 40348–40354, 40359–40366), seven adult males, eight adult females and a juvenile collected with the holotype by the same collectors, between 15 November and 19 November 2017. MZUSP A159552 (field number MTR 40321), an adult female from the base camp at "Bacia do Gelo", in the highlands of the Serra da Neblina, Parque Nacional do Pico da Neblina, Santa Isabel do Rio Negro, Amazonas State, Brazil (0.79286 N, 66.02500 W; 2,013 m a.s.l; map datum WGS84), collected on 22 November 2017; MZUSP A159556 (field number MTR 40330), an adult female from the trail to Pico da Neblina summit, close to "Pepita camp", in the highlands of the Serra da Neblina, Parque Nacional do Pico da Neblina, Santa Isabel do Rio Negro, Amazonas State, Brazil (0.79894 N, 66.01050 W; 2,330 m a.s.l; map datum WGS84); seven individuals, MZUSP A159553–A159555, MZUSP A159573–A159576 (field numbers MTR 40327–40329, MTR 40355–40358), three male and four females from the trail to Pico da Neblina summit, in the highlands of the Serra da Neblina, Parque Nacional do Pico da Neblina, Santa Isabel do Rio Negro, Amazonas State, Brazil (0.80011 N, 66.00989 W; 2,707 m a.s.l; map datum WGS84); seven individuals, MZUSP A159557–A159563 (field numbers MTR 40332–40338), five males and two females from the Pico da Neblina summit, Serra da Neblina, Parque Nacional do Pico da Neblina, Santa Isabel do Rio Negro, Amazonas State, Brazil (0.79992 N, 66.00750 W; 2,995 m a.s.l; map datum WGS84); all collected on 21 November 2017 by the same collectors as the holotype.

Etymology. The specific epithet *mayeri* is a noun in the genitive case, honoring General Sinclair James Mayer from the division "Sistema Defesa, Indústria e Academia" (SisDIA) of the Brazilian Army for his tireless work to provide logistical support and make the expedition to Pico da Neblina possible. Since then, General Mayer has promoted collaborations between the Army and our research group at the University of São Paulo, an effort that has already led to the collection of several species new to science from remote sites in Amazonia.

Definition. A minute brachycephaloid frog characterized by: (1) maximum SVL 19.2 mm in males and 20.1 mm in females (Table 1); (2) head narrower than body; (3) tympanic membrane and annulus absent, columella present; (4) frontoparietal smooth, cranial crests absent; (5) dentigerous process of vomer absent, vomers free of contact with any other bone; (6) subgular vocal sac conspicuous in some males although poorly defined (sometimes undetectable) in others, vocal slits present in males, located posterolaterally; (7) fingers fully developed, robust, tapering toward the tip, finger tips not expanded, rounded or slightly pointed on fingers I, II and IV, mucronate on Finger III, without discs and circumferential grooves, terminal phalanges pointed; (8) Finger I slightly shorter than Finger II; relative lengths of fingers: I < II < IV < III; nuptial pads absent; (9) Toes fully developed, robust, tapering toward the tip, toe tips not expanded, pointed or rounded on toes I and V, mucronate on toes II–IV, terminal phalanges pointed on toes I–II and knobbed on toes II–V; (10) relative lengths of toes: I < II < III< V <IV, Toe V only slightly longer than Toe III; (11) lateral fringes and webbing absent on fingers and toes; (12) subarticular tubercles small, round, not projecting; supernumerary tubercles absent; (13) outer metatarsal tubercule round, large and protruding, inner metatarsal tubercule ovoid, flat; (14) dorsolateral folds absent; (15) discoidal fold absent; (16) septomaxillae absent or highly vestigial; (17) iris dark brown in life; (18) *m. iliacus externus* originating via a single head anteriorly and extending in parallel alongside the entire length of the iliac shaft; (19) *m. tensor fasciae latae* originating anteriorly on the iliac shaft, immediately posterior to the sacral diapophyses (Supplementary Fig. S5).

Morphological comparisons with other Brachycephaloidea in the Pantepui biogeographical region. *Neblinaphryne* can be distinguished from all other brachycephaloid (in parentheses) by its pointed terminal phalanges (vs. T-shaped) and lack/highly vestigial state of septomaxillae (vs. present). It can be further distinguished from the four other brachycephaloid lineages occurring in Pantepui, i.e. *Adelophryne* (Eleutherodactylidae, Phyzelaphryninae), *Pristimantis* (Strabomantidae, Pristimantinae), *Ceuthomantis* (Ceuthomantidae) and *Dischidodactylus* (incertae sedis) as follows: from *Adelophryne* by its fully developed fingers and toes (vs. reduced FIV), with mucronate tips on FII and III and TII–IV only (vs. most fingers have mucronate tips) without lateral groove (vs. with groove); two subarticular tubercles on Finger IV (vs. single hump-shaped tubercule); lack of vomerine teeth (vs. present), and from *Ceuthomantis*, *Pristimantis* and *Dischidodactylus* by its mucronate tips on FII and III and TII–IV (vs. rounded); *m. tensor fasciae latae* originating anteriorly on the iliac shaft (vs. posterior or middle). It can further be distinguished from *Ceuthomantis* and *Dischidodactylus* by its *m. iliacus externus* originating anteriorly on the iliac shaft (vs. originating on the posterior half of the iliac shaft or on the posterior three-fourths of the iliac shaft), and from *Dischidodactylus* by the lack of vomerine teeth (vs. present).

Description of the holotype (Fig. 3). An adult female, SVL 20.1 mm; head slightly longer than wide, head length 37.3% SVL, head width 35.3% SVL; snout short, rounded in dorsal and lateral views (Fig. 1); width of upper eyelid 60.2% of interorbital distance; eye to nostril

distance 54.6% of eye diameter; nostrils ovoid, not protruding. Pupil horizontally oval. Canthus rostralis slightly concave. Tympanic membrane and annulus absent; head without enlarged tubercles or folds. Cranial crests and dentigerous processes of vomers absent. Vocal slits absent; vocal sac absent; tongue ovoid, free posteriorly for nearly half of its length; choanae small, round, located laterally and anteriorly. Skin on dorsum finely granular, without dorsolateral folds; skin on throat finely granular, areolate on belly; discoidal folds absent; cloacal sheath and tubercles absent. Fingers thin, short, without discs and circumferential grooves, lacking lateral fringes and webbing; fingertips not expanded, rounded or slightly pointed on fingers I, II and IV, mucronate on Finger III. Finger I slightly shorter than Finger II; Finger III long; relative lengths of fingers: I < II < IV < III. Subarticular tubercles on fingers not projecting, rounded (formula 1–1–2–2); supernumerary tubercles absent. Thenar tubercle ovoid, palmar tubercle round, larger than thenar. Nuptial pads absent. Fingers and toes slightly flattened ventrally; skin transparent on distal portion of fingers and toes. Toes without discs and circumferential grooves, toe tips not expanded, pointed or rounded on toes I and V, mucronate on toes II–IV, lacking lateral fringes and webbing. Toe V slightly longer than Toe III; relative lengths of toes: I < II < III < V < IV. Subarticular tubercles on toes rounded (formula 1–1–2–3–2); supernumerary tubercles absent. Inner metatarsal tubercle ovoid, flat. Outer metatarsal tubercle rounded, prominent, slightly larger than inner.

Measurements (in mm) of the holotype. SVL 20.1, HL 7.5, HW 7.1, IND 2.4, END 1.3, ED 2.4, EE 3.2, IOD 2.3, UEW 1.4, ARM 5.0, HAN 4.2, TH 8.8, TL 8.1, TAL 6.0, FTL 9.2.

Color of holotype in preservative. After five years in preservative, the general coloration of the holotype does not seem to have faded except for discolored blotches on dorsum, arms, and legs and scars coming from manipulation. The dorsum and dorsal surfaces of arms and legs are dark brown. Skin on articulations of fingers is lighter colored. Throat and ventral parts of arms, tibia and feet are dark brown. The ventral region from chest to thighs is light brown.

Variation in the type series (Supplementary Fig. S4). Males and females largely overlap in size (SVL 14.0–19.2 mm in males; 15.9–20.1 mm in females). Morphometric variation is summarized in Table 1. In two male paratypes (MZUSP A159562, SVL 16.7 mm; MZUSP A159574, SVL 14.7 mm), a subgular vocal sac is present (Supplementary Fig. S4) and vocal slits present, located posterolaterally. Vocal sacs and slits are absent in the remaining males. The background dorsal coloration in life is always brown, sometimes with irregular bluish-gray and red blotches on dorsal and lateral surfaces of head, body, and limbs (Fig. 3, Supplementary Fig. S4). A yellow transversal bar under the supratympanic fold may be present. Paracloacal yellow marks (in life, light gray in preservative) vary in position and size, sometimes extending on the posterior part of thighs. The background dorsal coloration in preservative varies little among individuals. However, a specimen has light gray dorsolateral lines (MZUSP A159570), and most have light gray blotches, of variable sizes, positioned in various places on the dorsum. A specimen (MZUSP A159557) has a light gray stripe below the supratympanic fold, anterior part of the arms, and a mid-dorsal line. Some specimens (e.g., MZUSP A159557) have bluish flecks on the flanks (white in preservative). Hands and fingers can have bluish and/or yellow marks too (MZUSP A159557, MZUSP A159570). Diffuse yellow pigmentation is also found on the posterior part of flanks in some specimens (e.g., the holotype) as well as on tarsus and feet. Background ventral coloration also varies little across specimens but comprises either diffuse yellow pigmentation (in life) that can be extensive (belly, upper arm, and thighs in MZUSP A159573) or limited to a few flecks (MZUSP A159558) or bluish flecks from throat to ventral sides of legs (MZUSP A159557, A159570) and does not seem related to the sex of the specimens.

The *m. iliacus externus* originates via a single head anteriorly and extends in parallel alongside the entire length of the iliac shaft (Supplementary Fig. S5). The *m. tensor fasciae latae* also originates anteriorly on the iliac shaft, immediately posterior to the sacral diapophyses (Supplementary Fig. S5). The characters correspond respectively to the state 2 of the character 0 and the state 2 of the character 1 of Ospina-Sarria and Grant (2021).

Osteology. The following description is based on the segmented skeleton of MZUSP A159552 (female paratype, field number MTR 40321) (Figs 4–5).

Cranium. The skull is of moderate size, widest at mid-length of the quadratojugal and slightly longer than wide (medial length ca. 104% of longest width). The braincase is moderately ossified; the sphenethmoid complex is moderately ossified, dorsally invested by the nasals only along its most anterior lateral margin. The prootic is widely separated laterally from the otic ramus of the squamosal and is in medial contact with the frontoparietal. Exoccipital and prootic are fused. The septomaxillae are not visible, but a tiny floating piece of bone between the nasal septum and the maxilla on the left side is likely a vestige of this delicate bone. The columellae (stapes) are well ossified, formed by the synostotic fusion of the long, thin pars media plectri (stylus) and the pars interna plectri (baseplate), which is curved.

Dorsal investing bones. The nasals are small, broadly separated. The posteromedial margin of the nasals is in short (right side), or point (left side) contact with the sphenethmoid, which has a straight anterior border that does not extend beyond the anterior margin of the orbit. The maxillary process of the nasal is long and acuminate but does not extend to the maxilla. The frontoparietal is smooth, free from exostosis. The frontoparietal completely roofs the central braincase from the anterior level of the orbit to the level of the *tectum synoticum* posteriorly. *Lamina perpendicularis* well developed along the entire orbital margin of the frontoparietal, expanding medially. No crests are visible on the frontoparietal. Prootic eminences partly decalcified. The occipital groove is fully invested by the posterior margin of the frontoparietal.

Ventral investing and palatal bones. The parasphenoid floors the braincase. The long, narrow rectangular cultriform process overlaps the sphenethmoid anteriorly and extends posteriorly from ca. mid-length of the sphenethmoid to the otic capsules. The parasphenoid alary processes provide the floor the otic capsules and are approximately perpendicular to the cultriform process. The posteromedial process of the parasphenoid reaches the margin of the *foramen magnum*. The lateral arms of the parasphenoid do not contact the highly reduced medial ramus of the pterygoid. The vomers are revealed as a pair of small floating bones with no visible osteological connection to either the sphenethmoid or the neopalatine. Postchoanal vomers absent; vomerine teeth absent. There is no visible connection between the neopalatine and the maxilla. The neopalatine is flat and slim, diagonally oriented, tapering towards the sphenethmoid.

Maxillary arcade. Both maxillae and premaxillae are dentate. The premaxillae are separated medially. The alary processes of the premaxillae are broad and rounded posteriorly, diverging from the midline, and are directed dorsally; in dorsal view the alary processes reach the level of the anteriormost margin of the maxilla. The palatine (medial) process of the premaxilla is long, slightly arcuate, rounded and directed posteriorly. The broad lateral process of the premaxilla is flat, similar in length to the palatine process and twice as wide as the medial process, truncate and directed posteriorly. The premaxillae appear to be co-ossified

to the maxillae. The maxilla is expanded, the *pars facialis* is well developed but does not contact the maxillary process of the nasal. Anteriorly, the *pars facialis* broadly overlaps the lateral margin of the *pars dentalis* of the premaxilla. The maxilla is short, strongly acuminate posteriorly, and lacks any posterodorsal projection directed towards the zygomatic ramus of the squamosal from which it is broadly separated. Posteriorly, the maxilla is broadly separated from the slim quadratojugal.

Suspensory apparatus. The pterygoid appears as rather reduced and barely triradiate. It bears a long, slim anterior ramus that is fused with the posterior end of the *pars palatina* of the maxilla. There is no visible contact with the squamosal. The posterior and medial rami are short and do not articulate with any other bone. The quadratojugal is short and slim and does not articulate with the maxilla. The squamosal does not articulate with any bone, except the quadratojugal. The otic and ventral rami of the squamosal are well developed; the otic ramus does not articulate with the prootic. The otic ramus bears a flange and is much longer than the zygomatic ramus. The zygomatic ramus is relatively short, bicuspid, and arcuate and acuminate in lateral profile. There is no contact with the maxilla.

Mandible. The dentary is short and slim, posteriorly acuminate, fused to the small, arcuate mentomeckelian anteriorly. The mentomeckelians are separated medially. The dentary overlaps the angulosplenial for ca. four fifth of its length (ca. one sixth of the angulosplenial length). The main component of the mandible is the angulosplenial, which is long and weakly sigmoid, acuminate anteriorly, and extends nearly to the mentomeckelian anteriorly. The coronoid process is dorsomedial and poorly developed. There is no mineralization in the hyoid corpus.

Postcranium. The vertebral column is composed of eight nonimbricate, procoelous presacral vertebrae, sacrum, and urostyle. The atlantal cotylar arrangement corresponds to the Type I of Lynch (1973). Presacrals II-V are stout and expand dorsally. The neural arches are well developed and bear large projecting neural crests on presacrals II-V. The transverse processes are moderately elongated, distally expanded on presacrals II-III only. The length of the transverse processes is III > IV > V = VI = VII = VIII > II. The transverse processes of presacral II are directed anteriorly and ventrally to the medial axis; those of presacral III are directed posteroventrally; transverse processes of presacral IV to VII are directed posterodorsally; and those of presacral VIII are directed roughly perpendicular to the medial axis. The sacral diapophyses are slightly flattened, not expanded distally and of similar length as the transverse processes of presacral III. The sacral diapophyses are directed posterodorsally, with truncate distal borders that are not in contact with the ilia distally. The sacrum has a bicondylar articulation with the urostyle. The urostyle is about the same length as the presacral vertebral column. It bears a well-developed dorsal crest along almost all its shaft. The crest starts anteriorly as a large, ossified tubercle and progressively decreases in height in the caudal direction.

The pectoral girdle is arciferal. The clavicles are slim, arcuate, directed anteriorly, and moderately separated from one another medially; the clavicle appears to be co-ossified to the scapula and attached to the coracoid. The posterior margin of the stout coracoid is weakly sigmoid, whereas the anterior margin is concave. The long axis of the coracoid is nearly perpendicular to the longitudinal axis of the body. The coracoids are separated and strongly expanded medially, the sternal end is about twice more expanded than the glenoid end, and slightly more than twice as wide as the midshaft width of the bone. The *pars acromialis* of the scapula appears to be paired with the *pars glenoidalis*. The cleithrum is a dagger-shaped element, the suprascapular cartilage is partly ossified. The head of the humerus is ossified.

There is a moderate *crista ventralis* extending along the proximal one fifth of the bone. The *cristae medialis* and *lateralis* are not evident in ventral (flexor) view. The capitulum and ulnar and radial condyles appear to be well developed. The olecranon of the radio-ulna is well developed, the *sulcus intermedius* is indicated by a distinct groove; the epiphyses of the radius and ulna appear to be ossified, as well as all carpal elements and the prepollex. The carpus is composed of a radiale, ulnare, ossified prepollex element, element Y, distal carpal 2 and an element representing the fusion of distal carpals 3–5 (dcpl 3–5). Both ulnare and dcpl 3–5 display a lateral apophysis on their anterodorsal border. The finger phalangeal formula is standard (2-2-3-3), and the metacarpals increase in size in the following order: I, IV, II and III. The relative lengths of the fingers increase in size in the following order: I, II, IV, III. The phalangeal elements are well ossified, the distal phalanges are slightly curved downwards and acuminate.

The postsacral trunk region is relatively short and narrow. The articulation between the anterior end of the ilial shafts and the ventral side of the distal ends of the sacral transverse processes is of the sagittal-hinge type (Reilly and Jorgensen, 2011), usually characteristic of long-distance jumpers. The ilial shafts have large crests along almost their full length, originating approximately at the level of the urostyle tubercle and terminating in a low posterior prominence. The ilia are posteriorly co-ossified to the ischium. The pubis appears as almost completely ossified; the acetabulum is round. The ischium possesses a short apophysis directed towards the urostyle. The femur and tibiofibula are approximately of equal length. The femur presents a slight sigmoidal curve and bears a low ventral ridge on its proximal end. The *sulcus intermedius* of the tibiofibula is less prominent than the *sulcus intermedius* of the radio-ulna. Presence of what appear to be a small graciella sesamoid and a large fabella sesamoid (Abdala et al., 2019). The astragalus and calcaneum are about two thirds the size of the tibiofibula. These structures are widely separated at their midpoint and fused at their distal and proximal heads. Presence of what appears to be a large cartilago sesamoid (Abdala et al., 2019). Two tarsals (distal tarsal 1 and an element representing the fusion of distal tarsals 2-3) are present at the base of digits I, II and III. An element Y and an elongate ossified prehallux element also appear to be present. A large lateral plantar sesamoid (Abdala et al., 2019) is present on the ventral surface of the pes. The toe phalangeal formula is standard (2-2-3-4-3), and the metatarsals increase in size in the following order: I, II, III, V, IV. The relative lengths of the toes increase in the same order. The phalangeal elements are mostly ossified, the toes distal phalanges appear to be similar to the fingers' distal phalanges, most having the tip slightly more knobbed compared to fingers.

Osteological variation (Figs 4–5, Supplementary Fig. S6). Except for changes due to demineralization, no significant differences were observed among the available µ-CT scanned specimens, except the presence of highly vestigial septomaxillae on both sides in MZUSP 159555 and MZUSP 159580 (vs. only one side in the holotype).

Distribution and natural history. All but one specimen of *Neblinaphryne mayeri* were found under rocks, where individuals often clustered together. Its large metatarsal tubercles suggest some degree of fossoriality. The surrounding habitat consisted of open grassy habitats with scattered short trees, or more frequently, steep rocky slopes. Specimens were sampled between 2,013 and 2,995 m asl, with the highest elevations corresponding to the summit of the Pico da Neblina, Brazil's highest mountain. Of the 33 specimens found, only two were collected below 2,600 m asl, at Bacia do Gelo (2,013 m) and at Pepita camp (2330 m). Despite our extensive use of pitfall and funnel traps at Bacia do Gelo, only one specimen was obtained through these methods. We heard no vocalization that could be attributed to this species during our field trip.

Class Amphibia Linnaeus, 1758

Order Anura Duméril, 1805

Superfamily Brachycephaloidea Günther, 1858

Caligophrynidae fam. nov.

Type genus: *Caligophryne* Fouquet, Kok, Recoder, Prates, Camacho, Marques-Souza, Ghellere, McDiarmid, Rodrigues, 2023

Diagnosis. The new family is distinguished from all other families within Hyloidea on the basis of molecular characters (see Fig. 2). It is considered a member of Brachycephaloidea based on molecular characters and the presence of arciferal pectoral girdles, partially fused calcanea and astragali, while lacking intercalary elements in the digits (Figs 7–8; Supplementary Fig. S6), and *m. iliacus externus* originating via a single head from the iliac shaft (Supplementary Fig. S5). We have not found any unambiguous phenotypic synapomophy for the family. However, it is unique by the combination of the following characteristics: (1) striking blue upper iris and concealed parts of legs black with small white flecks and dorsolateral black blotches (Fig. 6); (2) a massive, hyperossified skull with exostosed frontoparietal and parietal crests; (3) dentigerous process of vomer prominent, vomers co-ossified to sphenethmoid, neopalatines and nasals; (4) septomaxillae present; (5) terminal phalanges T-shaped (Figs 7–8; Supplementary Fig. S6; Table S3); (6) origin of *m. iliacus externus* with single head anteriorly, extending in parallel alongside almost the entire length of the iliac shaft; (7) origin of *m. tensor fasciae latae* on the anterior part of the iliac shaft (Supplementary Fig. S5).

Comparison with other families. No other Brachycephaloidea, except some *Strabomantis,* have such a hyperossified skull with exostosed frontoparietal and parietal crests. Moreover, the new family differs from any *Strabomantis* by having the vomers fused with the sphenethmoid, the neopalatines and the nasals. The new family further differs from those in the related family Brachycephalidae (*Ischnocnema* and *Brachycephalus*) in having a robust body and massive head, blue iris, crested frontoparietal, and squamosal and quadrojugal fused with maxilla (Supplementary Table S3).

Content. One genus, *Caligophryne* gen. nov.

Distribution. Known only from the Neblina massif, Pantepui, northeastern South America

***Caligophryne* gen. nov.**

Type species: *Caligophryne doylei* Fouquet, Kok, Recoder, Prates, Camacho, Marques-Souza, Ghellere, McDiarmid, Rodrigues, 2023

Diagnosis. Caligophrynidae being monotypic, the diagnosis of the genus is the same as for the family.

Content. One species, *Caligophryne doylei* sp. nov.

Distribution. Known only from the Neblina massif, Pantepui, northeastern South America.

Etymology. The generic name is formed by "*caligo*", a Latin word for "mist", and "*phryne*", a word meaning "toad" in Ancient Greek.

***Caligophryne doylei* sp. nov.**

leptodactylid sp. nov. McDiarmid and Cocroft *in* Brewer-Carías 1988: 668

Leptodactylid sp. McDiarmid and Donnelly 2005: 514

Holotype. MZUSP A159537 (field number MTR40255; Fig. 6), an adult male from the base camp at "Bacia do Gelo", in the highlands of the Serra da Neblina (Fig. 1), Parque Nacional do Pico da Neblina, Santa Isabel do Rio Negro, Amazonas State, Brazil (0.79286 N, 66.02500 W; 2,013 m a.s.l; map datum WGS84); collected on 15 November 2017 by M. T. Rodrigues, A. Camacho, F. Dal Vechio, I. Prates, J. M. Ghellere, R. Recoder and S. Marques-Souza.

Paratypes (n = 21) (Supplementary Fig. S4). Six males, MZUSP A159551, A159532–A159534, A159539, A159543 (field numbers MTR 40229, 40239, 40241, 40246, 40258, 40281); eight females, MZUSP A159530, A159531, A159535, A159536, A159538, A159540, A159541, A159546 (field numbers MTR 40230, 40232, 40247, 40248, 40256, 40260, 40264, 40306); and three juveniles, MZUSP A159542, A159544, A159545 (field numbers MTR 40275, 40288, 40291); collected with the holotype by the same collectors, between 15 November and 19 November 2017. A male, MZUSP A159547 (field number MTR 40331), from "Pepita", in the highlands of the Serra da Neblina, Parque Nacional do Pico da Neblina, Santa Isabel do Rio Negro, Amazonas State, Brazil (0.77622 N, 66.01600 W; 2.010 m a.s.l; map datum WGS84); collected on 19 November 2017, and one male MZUSP A159548 (field number MTR40341) and two females, MZUSP A159549–A159550 (field numbers MTR 40342–40343), from the trail to Pico da Neblina summit, in the highlands of the Serra da Neblina, Parque Nacional do Pico da Neblina, Santa Isabel do Rio Negro, Amazonas State, Brazil (0.79917 N, 66.01028 W; 2.600 m a.s.l; map datum WGS84), collected on 21 November 2017, by the same collectors as the holotype.

Referred specimens. Based on museum records, we were able to determine that several specimens of *C. doylei* were collected in the 1980s in the Venezuelan portion of the Neblina massif by two American-led expeditions. At least some of these specimens are now housed at the Smithsonian Institution (USA). Voucher information is as follows: USNM 562341 (field number RWM 17193), from Cerro de la Neblina, 2.8 km NE of Pico Phelps (= Pico Neblina), Camp II, state of Amazonas, Venezuela (coordinates on record 0.83333 N, 66.98000 W, clearly inaccurate; altitude on record ca. 2,100 m a.s.l.), collected on 17 February 1984 by R. W. McDiarmid; USNM 562349 (field number RWM 17287), same locality as USNM 562341, collected on 21 February 1984 by M. Foster; USNM 562352 (field number RWM 17647), from Cerro de la Neblina, 3.5 km NE of Pico Phelps (= Pico Neblina), Camp II, state of Amazonas, Venezuela (0.83333 N, 65.98000 W; ca. 2,100 m a.s.l.), collected on 29 January 1985 by R. W. McDiarmid; USNM 581819 (field number RWM 17648), a clutch of at least 11 eggs found right next to (and presumably laid by) USNM 562352. This egg clutch

was reared, subsampled, and preserved on 2 February 1984; vouchers USNM 581819–581823 correspond to the resulting developmental series.

Etymology. The specific epithet *doylei* is a noun in the genitive case, honoring Sir Arthur Conan Doyle for his influential novel "The Lost World", in which he depicted ancient creatures surviving until the present era on the isolated summit of a remote table-top mountain, like the frog we describe here.

Definition. A medium-sized brachycephaloid frog characterized by: (1) maximum SVL 29.6 mm in males and 33.8 mm in females (Table 1); (2) body robust and head massive; (3) tympanic membrane and annulus present, columella present; (4) frontoparietal exostosed and parietal crests present; (5) dentigerous process of vomer prominent, vomers fused with sphenethmoid, neopalatines and nasals; (6) vocal sac subgular, lateral vocal slits in males; (7) fingers fully developed, long, finger tips slightly expanded, rounded, without discs and circumferential grooves, terminal phalanges T-shaped; (8) Finger I longer than Finger II; relative lengths of fingers: II < IV < I < III; translucid rugous nuptial pads present on first phalange of FI in males; (9) toes fully developed, long, toe tips slightly expanded, rounded, terminal phalanges knob-shaped; (10) relative lengths of toes I < II < V < III < IV, Toe III slightly longer than Toe V; (11) lateral fringes absent on fingers and toes; (12) subarticular tubercles small, round, supernumerary tubercles present on hand, absent on feet; (13) outer metatarsal tubercle ovoid and protruding, inner metatarsal tubercle ovoid, larger than outer and protruding; (14) dorsolateral folds present; (15) discoidal fold present; (16) septomaxillae present; (17) color of the upper part of the iris in life blue with black reticulations; (18) origin of the *m. iliacus externus* with single head anteriorly, extending in parallel alongside almost the entire length of the iliac shaft; (19) origin of the *m. tensor fasciae latae* on the anterior part of the iliac shaft (Supplementary Fig. S5).

Morphological comparisons with other Brachycephaloidea of the Pantepui biogeographical region. *Caligophryne* can be distinguished from most other brachycephaloid (in parentheses) by its exostosed frontoparietal and parietal crests (vs. only present in *Strabomantis*). It can be further distinguished from the five other brachycephaloid lineages that occur in Pantepui, *i.e., Adelophryne* (Eleutherodactylidae, Phyzelaphryninae), *Pristimantis* (Strabomantidae, Pristimantinae), *Ceuthomantis* (Ceuthomantidae), *Dischidodactylus* (incertae sedis) and *Neblinaphryne* (Neblinaphrynidae), as follows: from *Adelophryne* by its fully developed fingers and toes (vs. reduced FIV), with rounded tips without lateral groove (vs. mucronate with grooves); two small subarticular tubercles on Finger IV (vs. single hump-shaped tubercle); and from *Ceuthomantis*, *Pristimantis* and *Dischidodactylus* by its *m. tensor fasciae latae* originating anteriorly on the iliac shaft (vs. posteriorly or medially). It can further be distinguished from *Ceuthomantis* and *Dischidodactylus* by its *m. iliacus externus* originating anteriorly of the iliac shaft (vs. originating on the posterior half of the iliac shaft or in the posterior three-fourths of the iliac shaft).

Description of the holotype (Fig. 5). An adult male, SVL 22.3 mm; head narrower than body, slightly wider than long, head length 39.9% SVL, head width 40.4% SVL. Snout moderately short, acutely rounded in dorsal view, rounded to nearly acuminate in lateral view; eye to nostril distance nearly equal in length to eye diameter; Upper eyelid bearing numerous small tubercles; width of upper eyelid 81.3% of interorbital distance; cranial crests indistinct. Pupil horizontally oval, upper part of iris bright blue with black reticulations, darker on the lower part. Canthus rostralis distinct, slightly curved in dorsal view, loreal region concave; nostrils small, rounded, slightly protruding. Tympanic membrane and annulus present,

tympanum nearly round, its length about one half the length of the eye; supratympanic fold well defined, extending from the posterior edge of the eye along the upper temporal region to the insertion of the arm. A pair of small and inconspicuous postrictal tubercles present. Choanae round; dentigerous processes of vomers prominent, ovoid, in transverse row posteromedially to the choanae. Vocal slits present; vocal sac single, median, and subgular; tongue large, elliptical. Skin on dorsum tuberculate, with dorsolateral folds, and scattered low warts; skin on throat finely granular, coarsely areolate on belly; ill-defined discoidal folds present; a short cloacal sheath present, cloacal tubercles absent. Fingers thin, moderately long, Finger I longer than Finger II; relative lengths of fingers: II < IV < I < III. Fingertips slightly expanded, rounded, without discs and circumferential grooves, lacking lateral fringes and webbing. Subarticular tubercles on fingers projecting, rounded (formula 1–1–2–2); supernumerary tubercles present. Thenar and palmar tubercles ovoid, subequal in length. Small, white ulnar tubercles forming a low ridge along the ventrolateral edge of the forearm. Nuptial pads absent. Toes thin and long, Toe III slightly longer than Toe V; relative lengths of toes: I < II < V < III < IV. Toes without discs and circumferential grooves, with slightly enlarged and rounded tips; narrow lateral fringes are present on toes, webbing absent. Subarticular tubercles on toes rounded (formula 1–1–2–3–2); supernumerary tubercles absent. Inner and outer metatarsal tubercles oval, nearly the same size. Small and white tarsal tubercles present, forming a low ridge on the outer edge of the tarsus; a minute conical tubercle present on the heel.

Measurements (in mm) of the holotype. SVL 22.3, HL 8.9, HW 9.0, IND 2.2, END 2.5, ED 2.7, EE 4.3, IOD 2.5, UEW 2.1, TD 1.4, ARM 4.6, HAN 5.3, TH 10.0, TL 9.6, TAL 6.0, FTL 9.3.

Color of holotype in life (Fig. 6). Dorsum dark brown with ill-defined and irregular light brown blotches. Interorbital region with a light brown W-shaped mark delimiting anteriorly a dark brown W-shaped scapular mark. Iris blue. Upper eyelid cream. Posterior part of the loreal region, below the eye and the tympanic region, reddish. Dark brown band from snout to eye along the dorsal part of the loreal region and posteriorly to the eye along the supratympanic fold. Flanks delimited by an ill-defined dorsolateral light brown band. Conspicuous black blotch surrounded by lighter brown below the dorsolateral line at the midbody level. Axillary region, upper and lower arm similarly colored as dorsum. Dorsal color of legs similar to that of dorsum. Concealed parts of legs and groin black with numerous white-bluish flecks. Throat background dark gray covered with minute black and light gray flecks. Anterior part of the belly as throat; posterior part of the belly orangish with scattered dark gray flecks. Ventral surfaces of thighs and arms as belly.

Color of holotype in preservative (Fig. 6). After five years in preservative, the general color of the holotype has faded. The general dorsal coloration became light brown. The loreal and tympanic region as well as the dorsolateral line became white. Conspicuously colored concealed part of the legs is now black with white flecks. Belly coloration is cream colored peppered with brown flecks that become denser anteriorly, particularly on anterior flanks and throat.

Variation in the type series (Supplementary Fig. S4). Males and females largely overlap in size although some females attain larger sizes (SVL 19.7–29.6 mm in males; 18.8–33.8 mm in females). Morphometric variation is summarized in Table 1. The species is highly polychromatic (Supplementary Fig. S4). The most remarkable variations across specimens are: dorsal coloration varies from light to dark brown to reddish in life (light brown in preservative, e.g., MZUSP A159548) with gray dorsal lines following the rows of tubercles

(MZUSP A159531), sometimes with bronze blotches (MZUSP A159535); the loreal region varies from white to reddish (holotype); the dorsolateral black blotches can be abundant and distributed on the scapular region (MZUSP A159550), along the flanks, or even absent (MZUSP A159548), although the occurrence of a single blotch below the dorsolateral line at the midbody level (holotype) is the most common pattern. Ventral coloration varies from yellow in life (whitish in preservative, e.g., MZUSP A159550) with relatively little dark pigmentation to being almost uniformly dark gray with lighter flecks (MZUSP A159549).

The *m. iliacus externus* originates via a single head anteriorly and extends in parallel alongside almost the entire length of the iliac shaft (Supplementary Fig. S5). The *m. tensor fasciae latae* originates anteriorly on the iliac shaft (Supplementary Fig. S5). The characters correspond respectively to the state 2 of the character 0 and the state 2 of the character 1 of Ospina-Sarria and Grant (2021).

Osteology. The following description is based on the segmented skeleton of MZUSP A159536 (male paratype, field number MTR40248) (Figs 7–8).

Cranium. The skull is massive, hyperossified, widest at mid-length of the quadratojugal and slightly wider than long (longest width ca. 110% of medial length). The braincase is well ossified; the sphenethmoid complex is ossified, invested by the nasals along the entire anterior margin. The prootic is overlapped laterally by the otic ramus of the squamosal and is in medial contact with the frontoparietal. Exoccipital and prootic are fused. The paired septomaxillae are well developed and lie dorsal to the palatine process and posterolaterally to the articulation between the maxilla and premaxilla. The columellae (stapes) are well ossified, formed by the synostotic fusion of the long, thin pars media plectri (stylus) and the pars interna plectri (baseplate), which is curved.

Dorsal investing bones. The nasals are broad, medially fused, posteriorly exostosed. The posteromedial margin of the nasals fully invests the sphenethmoid, which projects anteriorly in front of the anterior border of the nasals. The maxillary process of the nasal is large, acuminate, fused with the maxilla. Most of the frontoparietal is exostosed (covered with bony growths). The frontoparietal completely roofs the central braincase from the anterior level of the orbit to the level of the *tectum synoticum* posteriorly. *Lamina perpendicularis* well developed along the entire orbital margin of the frontoparietal, expanding posteriorly. The frontoparietal expands posterolaterally to form a low supraorbital crest that extends dorsally – as a parietal crest – along the medial margin of the anterior epiotic eminence towards about one third of the length of the posterior epiotic eminence. A low, continuous transverse crest (frontoparietal dorsal process) lies between the parietal crests, slightly anterior to the junction between the anterior and posterior epiotic eminences. The occipital groove is fully invested by the posterior margin of the frontoparietal.

Ventral investing and palatal bones. The parasphenoid forms the floor of the braincase. The long, broad cultriform process appears to be co-ossified to the sphenethmoid anteriorly and narrows posteriorly from the vomers to the otic capsules. The parasphenoid alary processes completely floor the otic capsules and are approximately perpendicular to the cultriform process. The posteromedial process of the parasphenoid is broadly acuminate and reaches the margin of the *foramen magnum*. The lateral arms of the parasphenoid are broadly in contact with the long medial ramus of the pterygoid. The vomers appear to be co-ossified to the sphenethmoid and the massive neopalatine. Arcuate postchoanal vomers are clearly

distinguishable, in broad contact with the neopalatine, each vomer bearing 7–8 teeth. There is a connection between the neopalatine and the maxilla on the inner surface of the latter.

Maxillary arcade. Both maxillae and premaxillae are dentate. The premaxillae are separated medially. The alary processes of the premaxillae are broad and acuminate posteriorly, diverging from the midline, and are directed posterodorsally; in dorsal view they fail to reach the level of the anteriormost margin of the maxilla. The palatine (medial) process of the premaxilla is long, slightly arcuate, acuminate and directed posterodorsally; it bears a flange on its ventral face. The narrow lateral process of the premaxilla is flat, about two third the length of the palatine process and as wide as the medial process, truncate and directed posteriorly. The premaxillae appear to be co-ossified to the maxillae. The maxilla is greatly expanded, the *pars facialis* is well developed and fused with the maxillary process of the nasal. Anteriorly, the *pars facialis* broadly overlaps the lateral margin of the *pars dentalis* of the premaxilla. The maxilla possesses a posterodorsal projection directed towards the zygomatic ramus of the squamosal with which it is co-ossified. Posteriorly, the maxilla is co-ossified to the robust quadratojugal. In lateral view the maxilla is pointed anteriorly.

Suspensory apparatus. The triradiate pterygoid is robust and bears an anterior ramus that anteriorly splits in two small branches, one is fused with the posterior end of the *pars palatina* of the maxilla, the other one appears to be fused with the *pars facialis*. The posterior ramus is broad and flat and appears to be co-ossified to the ventral ramus of the squamosal. The long medial ramus is in broad contact with the lateral arm of the parasphenoid and the prootic. The posterior and medial rami are of approximately equal length. The quadratojugal is robust and co-ossified to the maxilla. The otic and ventral rami of the squamosal are well developed; the otic ramus extends over the lateral margin of the prootic and onto its dorsal surface. The ventral ramus of the squamosal is broad and extends from the quadratojugal to the posterodorsal margin of the orbit. The otic ramus bears a flange and is longer than the zygomatic ramus. The zygomatic ramus is short and acuminate in lateral profile, co-ossified to the posterodorsally projected maxilla. The otic and zygomatic rami as well as the posterodorsal projection of the maxilla are weakly exostosed.

Mandible. The dentary is short and slim, posteriorly acuminate, fused to the small, arcuate mentomeckelian anteriorly. The mentomeckelians are separated medially. The dentary overlaps the angulosplenial for ca. three fourth of its length (ca. one sixth of the angulosplenial length). The main component of the mandible is the angulosplenial, which is long and sigmoid, acuminate anteriorly, and extends nearly to the mentomeckelian anteriorly. The coronoid process is dorsomedial and well-developed, about one third of the posterior ramus. There is no mineralization in the hyoid corpus.

Postcranium. The vertebral column is composed of eight nonimbricate, procoelous presacral vertebrae, sacrum, and urostyle. The atlantal cotylar arrangement corresponds to the Type I of Lynch (1973). Presacrals I–III are stout and expand dorsally. The neural arches are well developed and bear large projecting neural crests on presacrals II–III. The transverse processes are moderately elongated, distally expanded on presacral III only. The length of the transverse processes is III > II > IV > V > VII > VI = VIII. The transverse processes of presacral II are directed roughly perpendicularly and ventrally to the medial axis; those of presacral III are directed posteroventrally; transverse processes of presacral IV to VII are directed posterodorsally; and those of presacral VIII are directed perpendicular to the medial axis. A remarkable feature of the vertebral column is the presence of extensive paired calcified processes (possibly calcified endolymphatic sacs; Dempster, 1930) extending through the intervertebral foramina and under the transverse processes of vertebrae, shielding

the ventral surface of the vertebral column, starting from presacral III. These calcified processes extend under the sacrum and project posteriorly along the ilium as two claw-like protuberances reaching the posterior margin of the *tuber superius*. The sacral diapophyses are slightly flattened, distally expanded and of similar length as the transverse processes of presacral III. The sacral diapophyses are directed posterodorsally, with truncate distal borders in contact with the ilia distally. The sacrum has a bicondylar articulation with the urostyle and bears a pair of bony excrescences posteromedially. The urostyle is about the same length as the presacral vertebral column. It bears a well-developed dorsal crest along almost all its shaft. The crest starts anteriorly as a large, ossified tubercle and progressively decreases in height in the caudal direction.

The pectoral girdle is arciferal. The clavicles are robust, arcuate, directed anteriorly, and moderately separated from one another medially; the clavicle appears to be co-ossified to the scapula and attached to the coracoid. The posterior margin of the stout coracoid is weakly sigmoid, whereas the anterior margin is concave. The long axis of the coracoid is nearly perpendicular to the longitudinal axis of the body. The coracoids are separated and expanded medially, the glenoid and sternal ends are about equally expanded and slightly more than twice as wide as the midshaft width of the bone. The *pars acromialis* of the scapula appears to be paired with the *pars glenoidalis*. The cleithrum is a dagger-shaped element, the suprascapular cartilage is partly ossified. The head of the humerus is ossified. There is a moderate *crista ventralis* extending along the proximal half of the bone. The *cristae medialis* and *lateralis* are not evident in ventral (flexor) view. The capitulum and ulnar and radial condyles appear to be well developed. The olecranon of the radio-ulna is well developed, the *sulcus intermedius* is indicated by a distinct groove; the epiphyses of the radius and ulna appear to be ossified, as well as all carpal elements and the prepollex. The carpus is composed of a radiale, ulnare, ossified prepollex element, element Y, distal carpal 2 and an element representing the fusion of distal carpals 3–5 (dcpl 3–5). Both ulnare and dcpl 3–5 display a lateral apophysis on their anterodorsal border. The finger phalangeal formula is standard (2-2-3-3), and the metacarpals increase in size in the following order: I, IV, II and III. The relative lengths of the fingers increase in size in the following order: II, IV, I, III. The phalangeal elements are well ossified, the distal phalanges are slightly curved downwards and abruptly decrease in diameter at half of their length, with a thin column-shaped tip (but see Osteological variation below).

The postsacral trunk region is relatively short and narrow. The articulation between the anterior end of the ilial shafts and the ventral side of the distal ends of the sacral transverse processes is of the sagittal-hinge type (Reilly and Jorgensen 2011), usually characteristic of long-distance jumpers. The ilial shafts have large crests along almost their full length, originating approximately at the level of the urostyle tubercle and terminating in a posterior prominence. The ilia are posteriorly fused to the ischium. The pubis is not completely ossified; the acetabulum is round. The ischium possesses a short, flat dorsal projection directed towards the urostyle. The femur and tibiofibula are approximately of equal length. The femur presents a slight sigmoidal curve and bears a ventral ridge on its proximal end. The *sulcus intermedius* of the tibiofibula is less prominent than the *sulcus intermedius* of the radio-ulna. Presence of what appears to be a very small graciella sesamoid; fabella sesamoid not visible (Abdala et al., 2019). The astragalus and calcaneum are about half the size of the tibiofibula. These structures are widely separated at their midpoint and fused at their distal and proximal heads. Presence of what appears to be a very small cartilago sesamoid (Abdala et al., 2019). Two tarsals (distal tarsal 1 and an element representing the fusion of distal tarsals 2-3) are present at the base of digits I, II and III. An element Y and an elongate ossified prehallux element are also present. A very small lateral plantar sesamoid (Abdala et

al., 2019) is present on the ventral surface of the pes. The toe phalangeal formula is standard (2-2-3-4-3), and the metatarsals increase in size in the following order: I, II, III, V, IV. The relative lengths of the toes increase in the same order. The phalangeal elements are mostly ossified, the toes distal phalanges appear to be similar to the fingers' distal phalanges but with a rounder tip.

Osteological variation (Figs 7–8, Supplementary Fig. S6). Except for changes presumably due to demineralization, no significant differences were observed among the available µ-CT scanned specimens. The holotype (MZUSP A159537) is highly decalcified and was not used for formal osteological comparisons, but we note that it has no calcified processes under the transverse processes of vertebrae. Although the distal phalange is sometimes column-shaped (e.g., MZUSP A159536, see above), we assume that this condition is due to decalcification and/or µCT-scanning resolution as it is clearly T-shaped in MZUSP A159548. The prepollex is variable in size, reaching a substantial size in MZUSP A159548.

Distribution and natural history. While *Neblinaphryne mayeri* was more frequent at elevations above 2,600 m, *Caligophryne doylei* was mostly found at elevations around 2,000 m. Among the 22 specimens collected, most (N = 18) were found in open grassy habitats with scattered short trees around our camp at Bacia do Gelo. Three individuals were found at about 2,600 m, in the same open habitats where most *N. mayeri* specimens were sampled (Fig. 1, Supplementary Figs S1–2). A single specimen was captured in a funnel trap; all others were hand-captured. We heard no vocalization that could be attributed to this species during our field trip. We note that one specimen collected in 1984 on the Venezuelan side of the Neblina massif (USNM 562352) was found sitting next to, and seemingly guarding, a clutch of at least 11 round whitish eggs on wet moss (USNM records and R.W. McDiarmid, personal observation). This observation confirms direct development and suggests parental care in *C. doylei*.

4. Discussion

4.1. Systematics of Brachycephaloidea

Supraspecific Linnaean ranks have no inherent biological meaning except that only monophyletic taxa should be named (e.g., Forey et al., 2004; Orthia et al., 2005; Wiley and Lieberman, 2011). Therefore, there is often a subjective component in supraspecific classification because several monophyly-grounded classifications can be available and thus some additional criteria have to be considered to provide practical taxa and avoid unnecessary nomenclatural actions. Some criteria have been summarized and hierarchized by Vences et al. (2013), notably clade stability and phenotypic diagnosability, as well as time banding and biogeography.

Our two new genera and families are monotypic. Some authors have claimed that monotypic classification units should be avoided (e.g., Farris, 1976; Wiley, 1979) because they contribute to the proliferation of taxon names that identify no supraspecific clades. However, monotypic supraspecific categories can sometimes be appropriate to designate phylogenetically deeply divergent taxa, particularly relict ones exhibiting high phenotypic diagnosability, such as the frog lineages considered here.

In the case of *Neblinaphryne*, the erection of a new family and a new genus is the most economical taxonomic action possible, since this taxon is the sister group of several distinct families and many genera. Moreover, this hypothesis is supported by (1) phenotypic diagnosability (in particular the absence/highly vestigial state of septomaxillae) as well as (2) deep time of divergence from other Brachycephaloidea, except *Ceuthomantis*, of ca. 55 Ma (i.e., older than the crown age of many Hyloidea families).

In the case of *Caligophryne*, the taxon is the sister group of a single and diverse family (Brachycephalidae, 78 species) restricted to the Atlantic Forest domain, and could have thus been assigned as a new genus within this family. However, we prefer to keep the current composition of Brachycephalidae, and consider that the (1) phenotypic diagnosability of *Caligophryne* (as notably compared to *Brachycephalus* and *Ischnocnema*), (2) biogeographic location and restriction (i.e., Pantepui endemic vs. coastal Atlantic Forest), and (3) deep time of divergence from its sister group, Brachycephalidae, of ca. 45 Ma (i.e., older than the crown age of many Hyloidea families) justify the erection of a new family.

With >1200 species described and hundreds remaining undescribed (e.g., Taucce et al., 2018; Páez and Ron, 2019; Catenazzi et al., 2020), Brachycephaloidea is by far the most species-rich lineage of amphibians and possibly of vertebrates of comparable age (60 My). The species within this group share direct development, i.e., lacking a free tadpole stage, and have diversified throughout the Neotropics, with many genera and families restricted to particular geographic regions and spectacular variation in species diversity across clades (e.g., some monotypic genera vs. *Pristimantis* with over 600 described species; Frost, 2023). Understanding the phylogenetic relationships and timing of diversification of major lineages in this clade can thus provide crucial insights into Neotropical biogeography. We recovered *Ceuthomantis* as the earliest diverging branch within Brachycephaloidea, in accordance with the phylogenomic studies of Heinicke et al. (2009, 2015, 2018), Pyron and Wiens (2011), Feng et al. (2017), Jetz and Pyron (2018), Hutter et al. (2017), Castroviejo et al. (2015), Motta et al. (2021), Dubois et al. (2021), Hime et al. (2021) and the results of the maximum likelihood analysis of Padial et al. (2014), with the exception of the poorly supported position of *Cryptobatrachus*. The topology of the latter contrasts with the results obtained in that same study (Padial et al. 2014) using a maximum parsimony analysis that involved a smaller genomic (but larger taxonomic) dataset and direct optimization. This method may fare poorly when dealing with variable-length ribosomal RNA sequences such as 12S and 16S (Ogden and Rosenberg, 2007; Kjer and Honeycutt, 2007). Therefore, the position of *Ceuthomantis* as the sister group of all the other Brachycephaloidea appears more likely.

Among major Brachycephaloidea lineages, we recovered Eleutherodactylidae and Brachycephalidae as sister groups using the concatenated mtDNA+nuDNA, agreeing with Jetz and Pyron (2018), Dubois et al. (2021) and Hutter et al. (2017). However, using nuDNA, we recovered (Brachycephalidae (Eleutherodactylidae (Craugastoridae + Strabomantidae))), which is in accordance with the phylogenomic studies of Pyron and Wiens (2011), Heinicke et al. (2015), Feng et al. (2017), Streicher et al. (2018), Barrientos et al. (2021), and Fouquet et al. (2022). This result also contradicts an earlier divergence of Eleutherodactylidae as found by Padial et al. (2014), Pie et al. (2017), Castroviejo et al. (2015), Heinicke et al. (2009, 2018), Motta et al. (2021) and Hime et al. (2021). We note that this last topology might have been driven mostly by signals coming from mtDNA data and potentially affected by saturation and long branch attraction (Yang, 2006; Cannarozzi and Schneider, 2012). Nevertheless, considering these conflictual results in previous work and ours, uncertainty remains concerning the exact phylogenetic relationships of Brachycephalidae and Eleutherodactylidae.

4.2. The evolution of Pantepui biota

Phylogenetic estimates of divergence times in amphibians have revealed astonishingly ancient lineages of frogs in South American mountains, such as the recently described Brachycephaloidea genera *Ceuthomantis* in Pantepui (Heinicke et al., 2009) and *Tachiramantis* in the northern Andes (Heinicke et al., 2015, 2018). Moreover, several other new genera of Brachycephaloidea have been described, being supported by high levels of molecular divergence (*Serranobatrachus* Arroyo et al., 2022; *Microkayla* De la Riva et al., 2018; *Qosqophryne* Catenazzi et al., 2020; and *Bahius* Dubois et al., 2021). While the old divergences of these genera (as revealed by genetic data) were somewhat unexpected, at least some of the species within each of them were collected and described by zoologists under pre-existing genera decades ago (e.g., *Serranobatrachus* and *Bahius*). In contrast, *Neblinaphryne* and *Caligophryne* represent two previously undescribed lineages of vertebrates from a single locality and whose morphological and genetic divergences are so deep that they justify the erection of two new taxonomic families. As such, these frogs provide a bewildering reminder of how incomplete our perception of Neotropical biodiversity remains. The discovery of *Neblinaphryne* and *Caligophryne* evokes that of *Nasikabatrachus* (Biju and Bossuyt, 2003) from India's mountainous Western Ghats region. The discovery of *Nasikabatrachus* revealed biogeographical links between the Indian subcontinent and the Seychelles archipelago. Similarly, the two new Pantepui taxa documented herein provide insights into the historical biography of the South American continent, as we discuss below.

All these recently described genera of Brachycephaloidea, as well as many other previously described genera in the clade, are associated with mountain ranges. It has been suggested that most mountain ranges can act both as cradles (promoting *in situ* speciation) and museums (hosting isolated relict species from groups that have gone extinct elsewhere) (Rahbek et al., 2019). *Ceuthomantis*, *Neblinaphryne* gen. nov. and *Caligophryne* gen. nov. (and possibly *Dischidodactylus*) are Pantepui frog genera that form the earliest diverging lineages within Brachycephaloidea, a clade that harbors almost half of the species (>1200 species) of Hyloidea (Padial et al., 2014; Heinicke et al., 2018; Barrientos et al., 2020). These relationships may suggest an early Cenozoic phase of diversification within the Pantepui region 60–50 Mya, in line with the Plateau theory (see Kok, 2013). Nevertheless, they originated at such an old time that the possible loss of lineages through extinction will inevitably keep this hypothesis speculative in the absence of fossils. An alternative hypothesis is that these Pantepui lineages represent relics that have survived along tepui slopes (as opposed to isolated on tepui tops) throughout the Cenozoic while going extinct in other northern South American regions.

Pantepui started to experience uplifts during the Cretaceous, notably during the Upper Cretaceous/Paleocene, close to the K-T boundary (Kok, 2013). The extent of this uplift is difficult to assess, but erosional denudation was probably extensive and could have substantially lowered the plateau during the Paleogene, making it suitable for a diverse paleofauna. That last uplift phase slightly predates (and possibly promoted) the split between *Ceuthomantis*, *Neblinaphryne* and *Caligophryne* from their respective sister lineages. Vertical isolation from the surrounding areas of the—already partly eroded—plateau would have likely reached its peak in the Middle Eocene and Oligocene (Kok, 2013), with some major massifs (e.g., Chimantá and Auyán-tepui) disconnected from each other, but several tepuis and tepui massifs still linked to each other and to adjoining uplands by more or less extensive ridges (remnants of which are still visible today; Kok 2013). That epoch (Middle Eocene and

Oligocene) roughly corresponds to the split between most known endemic Pantepui genera in other frog families from their respective sister groups (Kok, 2013).

Similar to *Neblinaphryne* and *Caligophryne*, early branching lineages from several other frog families occur in this region. This is the case of the endemic treefrog genera *Nesorohyla* and *Myersiohyla* (Hylidae). Mirroring the case of *Ceuthomantis*, *Caligophryne*, and *Neblinaphryne*, those two hylid genera are early branching relatives of a clade containing all the other Neotropical Cophomantini (Pinheiro et al., 2019), having diverged from other genera before 34 Ma (Feng et al., 2017; Hime et al., 2021). Other examples are the separation ca. 30 Ma of the endemic Pantepui genus O*reophrynella* (Bufonidae) from *Atelopus* (Andean origin) (Kok et al., 2018; Moraes et al., 2022) and of *Anomaloglossus* (Pantepui origin) from its Andean relatives (Vacher et al., in press). The only examples of similarly old diversifications are Otophryninae, which diversified within Pantepui ca. 55 Ma (Fouquet et al., 2021), and the hemiphractid genus *Stefania*, which is sister to the other genera of Hemiphractidae except for the clade formed by *Cryptobatrachus* and *Flectonotus* (Castroviejo et al., 2015) and having diverged ca. 40 Ma (Kok et al., 2017). Remarkably, the three endemic Brachycephaloidea genera are by far the most ancient Pantepui endemic lineages described to date.

These examples suggest that the relative stability and altitudinal gradients of Pantepui have favored the persistence of some lineages throughout the Cenozoic, regardless of whether they represent early in-situ diversification or relics of once more diversified and widespread lineages. During this long period, some species may have experienced range shifts up and down mountain slopes in response to climatic fluctuations, notably during those of the Quaternary, allowing them to persist through altitudinal shifts. This would be especially true within large massifs such as Neblina, but a less likely scenario for high tepui summit fauna. Indeed, such vertical migration promoted by recent climatic fluctuations was reported as not realistic for plant taxa occurring on the highest tepuis (i.e., those with a base-summit difference exceeding 1,100 m) because the maximum downward vertical shift of climatic zones estimated for the region during the last glaciation was 1,100 m (Rull, 2005). Similarly, vertical shifts of this magnitude may have been too extreme to allow movement of certain Pantepui herpetofauna along tepui slopes (Kok, 2013). Such restriction could explain (1) the ancient divergences recorded between summit populations of certain groups (e.g., Brachycephaloidea and *Stefania*), and (2) the absence of some typical Pantepui taxa from specific tepui tops (either due to extinction or the impossibility to disperse to these tops) (Kok, 2013). Nevertheless, we must be aware that current tepui isolation does not necessarily reflect the situation of the area a few million years ago (Kok, 2013), and the configuration of the Neblina massif differs from that of tabletop-shaped tepuis per se, with more gradual granitic slopes that could have harbored different vegetation types along the eons and favored the movement of species.

Whereas geologically active areas such as the Andes may have higher rates of speciation, older and more stable regions like the tepuis appear to have acted as evolutionary "refugia" or "museums". Early branching lineages like the two new frog families we have discovered can provide a wealth of data on ancient processes of landscape and evolutionary changes, like those that happened during the Paleogene. This source of biogeographic information is particularly important for groups whose fossil record is highly fragmentary, as is the case of Neotropical amphibians.

4.3. Conservation

Another important aspect of this discovery is that it strengthens the perception that the Guiana Shield highlands harbor a unique biodiversity that is deeply rooted in the tree of life and thus hosts high phylogenetic diversity. These lineages are highly threatened by the combination of their small spatial and altitudinal range and climate change, like for the vast majority of insular and highland species (Manes et al., 2021). Climate change is becoming one of the most significant threats to biodiversity (Smale et al., 2019; Trisos et al., 2020), and some studies suggest that climate-driven extinctions and range reductions are already widespread (Lister et al., 2018; Platts et al., 2019). These changes are expected to have greater impact in the tropics (Foden et al., 2013; Linck et al., 2021) given that tropical species often have narrower thermal tolerances than temperate species (Sheldon et al., 2011; Sunday et al., 2011). This is particularly true for ectotherms such as amphibians (Buckley et al., 2012; Duarte et al., 2012) because their basic physiology is dependent on environmental temperature and humidity (Blaustein and Wake, 1990; Sheldon et al., 2011). Shifts in altitudinal distribution have already been observed in Brachycephaloidea, potentially related to changes in precipitation or increasing temperature (Pounds et al., 1999; Burrowes et al., 2004). However, there is simply no higher ground for mountaintop specialized species, leaving no altitudinal shift possible (Courtois et al., 2016). An additional threat in Pantepui is the human mediated introduction of pathogens (such as chytridiomycosis) in immunologically naïve amphibian communities as demonstrated by Kok et al. (2022). Due to their restricted elevational range, the size of suitable habitat for these species does not extend beyond ca. 96 km^2 (Supplementary Fig. S7; i.e. matching IUCN's criteria B1). Moreover, this elevational range will presumably be reduced due to ongoing climate change (i.e. criteria B2, an area of occupancy unknown but most likely very small, single known population (a), and projected general decline (b)). Therefore, we suggest that these two new taxa should be considered Critically Endangered (IUCN).

Acknowledgements

We thank Generals Sinclair James Mayer, Geraldo Miotto (in memoriam), Omar Zendin and Eduardo Villas Boas, Colonel Alexsandro Henriques, Captains Jorge Leandro, Ronaldo José Piedade and all personnel of the Brazilian Army involved in planning and providing financial and logistical support during the Brazilian expedition to Pico da Neblina. We also thank Paulo Muzy from the University of São Paulo, Eloisa Cabral (SISDIA), the Yanomami community at Maturacá for their invaluable help during the expedition and Francisco Dal Vechio, Luis Fabio Silveira, Alexandre Percequillo and Renato de Mello-Silva (in memoriam) for assistance in the field. Addison Wynn and Steve Gotte provided information about the Venezuelan specimens of *C. doylei* housed at the Smithsonian Institution. Fundação de Amparo à Pesquisa do Estado de São Paulo (FAPESP 2011/50146-6, 2012/15754-8, 2017/08357-6) National Science Foundation [Dimensions of Biodiversity Program (NSF: DOB 1343578), (FAPESP: BIOTA 2013/50297-0), and NASA)], Coordenação de Aperfeiçoamento de Pessoal de Nível Superior [Capes]) and Conselho Nacional de Desenvolvimento Científico e Tecnológico (CNPq 301778/2015-9) provided financial support. This study benefited from an "Investissement d'Avenir" grant managed by the Agence Nationale de la Recherche (CEBA, rANR-10-LABX-25-01). The work of PJRK was supported by a Marie Skłodowska-Curie Actions (MSCA) grant (101022238/HOSTILE). Agustín Camacho was supported by a MSCA-Individual Fellowship (897901). We also warmly thank Lucie Moreau and Yves Cuenot for PCRs and library construction, Juliana

Tanaka, Manuel Antunes and Beatriz Freire for help in the lab, and Phillip Lenkaitis and Enio Mattos for CT-Scans.

References

Abdala, V., Vera, M.C., Amador, L.I., Fontanarrosa, G., Fratani, J., Ponssa, M.L., 2019. Sesamoids in tetrapods: the origin of new skeletal morphologies. Biological Reviews 94, 2011–2032.

Arroyo, S., Targino, M., Rueda-Solano, L.A., Daza, J.M., Grant, T., 2022. A new genus of terraranas (Anura: Brachycephaloidea) from northern South America, with a systematic review of *Tachiramantis*. Syst. Biodivers. 20(1), 2123865.

Azevedo, J.A., Guedes, T.B., Nogueira, C.D.C., Passos, P., Sawaya, R.J., Prudente, A.L., Barbo, F.E., Strüssmann, C., Franco, F.L., Arzamendia, V., Giraudo, A.R., 2020. Museums and cradles of diversity are geographically coincident for narrowly distributed Neotropical snakes. Ecography 43(2), 328–339.

Barrientos, L.S., Streicher, J.W., Miller, E.C., Pie, M.R., Wiens, J.J., Crawford, A.J., 2021. Phylogeny of terraranan frogs based on 2,665 loci and impacts of missing data on phylogenomic analyses. Syst. Biodivers. 19(7), 818–833.

Biju, S.D., Bossuyt, F., 2003. New frog family from India reveals an ancient biogeographical link with the Seychelles. Nature 425(6959), 711–714.

Boschman, L.M., Condamine, F.L., 2022. Mountain radiations are not only rapid and recent: Ancient diversification of South American frog and lizard families related to Paleogene Andean orogeny and Cenozoic climate variations. Glob. Planet. Change 208, p.103704.

Bouckaert, R., Heled, J., Kühnert, D., Vaughan, T., Wu, C.-H., Xie, D., Suchard, M.A., Rambaut, A., Drummond, A.J., 2014. BEAST 2: A software platform for Bayesian evolutionary analysis. PLoS Comput. Biol. 10, e1003537.

Cannarozzi, G.M., Schneider, A., 2012. Mechanisms and Models. Oxford University Press, Codon Evolution.

Castroviejo-Fisher, S., Guayasamin, J.M., Gonzalez-Voyer, A., Vilà, C., 2014. Neotropical diversification seen through glassfrogs. J. Biogeogr. 41, 66–80. https://doi.org/10.1111/jbi.12208

Castroviejo-Fisher, S., Padial, J. M., De La Riva, I., Pombal Jr, J.P., Da Silva, H.R., Rojas-Runjaic, F.J., Medina-Mendez, E., Frost, D.R., 2015. Phylogenetic systematics of egg-brooding frogs (Anura: Hemiphractidae) and the evolution of direct development. Zootaxa 4004(1), 1–75.

Catenazzi, A., Mamani, L., Lehr, E., von May, R., 2020. A new genus of terrestrial-breeding frogs (Holoadeninae, Strabomantidae, Terrarana) from southern Peru. Diversity 12(5), 184

Courtois, E.A., Michel, E., Martinez, Q., Pineau, K., Dewynter, M., Ficetola, G.F., Fouquet, A., 2016. Taking the lead on climate change: modelling and monitoring the fate of an Amazonian frog. Oryx 50(3), 450–459.

Brewer-Carías, C., 1988. Cerro de la Neblina. Resultados de la expedición 1983-1987. Fundación para el Desarrollo de las Ciencias Físicas, Matematicas y Naturales, Caracas, Venezuela

Chen, Y.W., Wu, J., Suppe, J., 2019. Southward propagation of Nazca subduction along the Andes. Nature 565(7740), 441–447.

Chernomor, O., Klaere, S., von Haeseler, A., Minh, B.Q., 2016. Split diversity: measuring and optimizing biodiversity using phylogenetic split networks. *in* Biodiversity Conservation and Phylogenetic Systematics: Preserving our evolutionary heritage in an extinction crisis, Pellens, R. Grandcolas, P. (Eds.), pp. 173–195. Springer.

De la Riva, I., Chaparro, J.C., Castroviejo-Fisher, S., Padial, J.M., 2018. Underestimated anuran radiations in the high Andes: five new species and a new genus of Holoadeninae, and their phylogenetic relationships (Anura: Craugastoridae). Zool. J. Linn. Soc. 182(1), 129–172.

Dempster, W.T., 1930. The morphology of the amphibian endolymphatic organ. J. Morphol. Physiol., 50, 71–126.

Dierckxsens, N., Mardulyn, P., Smits, G., 2017. NOVOPlasty: de novo assembly of organelle genomes from whole genome data. Nucleic acids res. 45(4), e18–e18.

Doyle, A.C., 1912. The lost world. London: Hodder & Stoughton.

Dubois, A., Ohler, A., Pyron, R.A., 2021. New concepts and methods for phylogenetic taxonomy and nomenclature in zoology, exemplified by a new ranked cladonomy of recent amphibians (Lissamphibia). Megataxa 5(1), 1–738.

Duméril, A.M.C., 1805. *Zoologie Analytique, ou Méthode Naturelle de Classification des Animaux, Rendue plus Facile à l'Aide de Tableaux Synoptiques*. Paris, Allais.

Drummond, A.J., Ho, S.Y.W., Phillips, M.J., Rambaut, A., 2006. Relaxed phylogenetics and dating with confidence. PLoS Biol 4, e88.

Duellman, W.E., Lehr, E. 2009. Terrestrial–breeding frogs (Strabomantidae) in Peru. Münster: Natur und Tier –Verlag GmbH.

Dunlap, D.G., 1960. The comparative myology of the pelvic appendage in the Salientia. J. Morphol. 106, 1–76.

Esquerré, D., Brennan, I.G., Catullo, R.A., Torres-Pérez, F., Keogh, J.S., 2019. How mountains shape biodiversity: The role of the Andes in biogeography, diversification, and reproductive biology in South America's most species-rich lizard radiation (Squamata: Liolaemidae). Evolution 73(2), 214–230.

Feng, Y.J., Blackburn, D.C., Liang, D., Hillis, D.M., Wake, D.B., Cannatella, D.C., Zhang, P., 2017. Phylogenomics reveals rapid, simultaneous diversification of three

major clades of Gondwanan frogs at the Cretaceous–Paleogene boundary. Proc. Natl. Acad. Sci. U.S.A. 114(29), E5864–E5870.

Fouquet, A., Réjaud, A., Rodrigues, M.T., Ron, S. R., Chaparro, J. C., Osorno, M., Werneck, F.P., Hrbek, T., Lima A.P., Camacho-Badani, T., Jaramillo-Martinez A.F., Chave, J., 2022. Diversification of the *Pristimantis conspicillatus* group (Anura: Craugastoridae) within distinct neotropical areas throughout the Neogene. Syst. Biodivers. 20(1), 2130464.

Fouquet, A., Leblanc, K., Framit, M., Réjaud, A., Rodrigues, M.T., Castroviejo-Fisher, S., Peloso, P.L. V, Prates, I., Manzi, S., Suescun, U., Baroni, S., Moraes, L.J.C.L., Recoder, R., de Souza, S.M., Dal Vecchio, F., Camacho, A., Ghellere, J.M., Rojas-Runjaic, F.J.M., Gagliardi-Urrutia, G., de Carvalho, V.T., Gordo, M., Menin, M., Kok, P.J.R., Hrbek, T., Werneck, F.P., Crawford, A.J., Ron, S.R., Mueses-Cisneros, J.J., Rojas Zamora, R.R., Pavan, D., Ivo Simões, P., Ernst, R., Fabre, A.-C., 2021. Species diversity and biogeography of an ancient frog clade from the Guiana Shield (Anura: Microhylidae: *Adelastes, Otophryne, Synapturanus*) exhibiting spectacular phenotypic diversification. Biol. J. Linn. Soc. 132, 233–256. https://doi.org/10.1093/biolinnean/blaa204

Fouquet, A., Loebmann, D., Castroviejo-Fisher, S., Padial, J.M., Orrico, V.G., Lyra, M.L., Roberto, I.J., Kok, P.J.R., Haddad, C.F., Rodrigues, M.T., 2012. From Amazonia to the Atlantic forest: Molecular phylogeny of Phyzelaphryninae frogs reveals unexpected diversity and a striking biogeographic pattern emphasizing conservation challenges. Mol. Phyl. Evol. 65(2), 547–561.

Frost, D.R., 2023. Amphibian Species of the World: an Online Reference. Version 6.2 (25 July 2023). Electronic Database accessible at https://amphibiansoftheworld.amnh.org/index.php. American Museum of Natural History, New York, USA. doi.org/10.5531/db.vz.0001

Garzione, C.N., Hoke, G.D., Libarkin, J.C., Withers, S., MacFadden, B., Eiler, J., Ghosh, P., Mulch, A., 2008. Rise of the Andes. Science 320(5881), 1304–1307.

Gentry, A.H., 1982. Patterns of neotropical plant species diversity. In Evolutionary biology (pp. 1–84). Springer, Boston, MA.;

Giam, X., Scheffers, B.R., Sodhi, N.S., Wilcove, D.S., Ceballos, G., Ehrlich, P.R., 2012. Reservoirs of richness: least disturbed tropical forests are centres of undescribed species diversity. Proc. Royal Soc. B 279(1726), 67–76.

Günther, A.C.L.G., 1858. Neue Batrachier in der Sammlung des britischen Museums. Archiv für Naturgeschichte. Berlin 24, 319–328.

Hammond, D.S., 2005. Tropical forests of the Guiana Shield: ancient forests in a modern world. Cambridge (MA): CABI publishing. p. 528.

Heinicke, M.P., Duellman, W.E., Trueb, L., Means, D.B., MacCulloch, R.D., Hedges, S.B., 2009. A new frog family (Anura: Terrarana) from South America and an expanded direct-developing clade revealed by molecular phylogeny. Zootaxa 2211(1), 1–35.

Heinicke, M.P., Barrio-Amoros, C.L., Hedges, S.B., 2015. Molecular and morphological data support recognition of a new genus of New World direct-developing frog (Anura: Terrarana) from an under-sampled region of South America. Zootaxa 3986(2), 151–172.

Heinicke, M.P., Lemmon, A.R., Lemmon, E.M., McGrath, K., Hedges, S.B., 2018. Phylogenomic support for evolutionary relationships of New World direct-developing frogs (Anura: Terraranae). Mol. Phyl. Evol. 118, 145–155.

Hime, P.M., Lemmon, A.R., Lemmon, E.C.M., Prendini, E., Brown, J.M., Thomson, R.C., Kratovil, J.D., Noonan, B.P., Pyron, R.A., Peloso, P.L. V, Kortyna, M.L., Keogh, J.S., Donnellan, S.C., Mueller, R.L., Raxworthy, C.J., Kunte, K., Ron, S.R., Das, S., Gaitonde, N., Green, D.M., Labisko, J., Che, J., Weisrock, D.W., 2021. Phylogenomics reveals ancient gene tree discordance in the amphibian tree of life. Syst. Biol. 70, 49–66. https://doi.org/10.1093/sysbio/syaa034

Hoorn, C., Bogotá-A, G.R., Romero-Baez, M., Lammertsma, E.I., Flantua, S.G., Dantas, E.L., Dino, R., do Carmo, D.A., Chemale Jr, F., 2017. The Amazon at sea: Onset and stages of the Amazon River from a marine record, with special reference to Neogene plant turnover in the drainage basin. Glob. Planet. Change 153, 51–65.

Hoorn, C., Wesselingh, F.P., ter Steege, H., Bermudez, M.A., Mora, A., Sevink, J., Sanmartín, I., Sanchez-Meseguer, A., Anderson, C.L., Figueiredo, J.P., Jaramillo, C., Riff, D., Negri, F.R., Hooghiemstra, H., Lundberg, J., Stadler, T., Särkinen, T., Antonelli, A., 2010. Amazonia through time: Andean uplift, climate change, landscape evolution, and biodiversity. Science 330, 927–931.

Huber, 0., 2005. Diversity of vegetation types in the Guayana Region: an overview. Biologiske Skrifter 55, 169

Hughes, C., Eastwood, R., 2006. Island radiation on a continental scale: exceptional rates of plant diversification after uplift of the Andes. Proc. Natl. Acad. Sci. U.S.A. 103(27), 10334–10339.

Hutter, C.R., Lambert, S.M., Wiens, J.J., 2017. Rapid diversification and time explain amphibian richness at different scales in the Tropical Andes, Earth's most biodiverse hotspot. Am. Nat. 190(6), 828–843.

Jenkins, C.N., Pimm, S.L., Joppa, L.N., 2013. Global patterns of terrestrial vertebrate diversity and conservation. Proc. Natl. Acad. Sci. U.S.A. 110(28), E2602–E2610.

Jetz, W., Pyron, R.A., 2018. The interplay of past diversification and evolutionary isolation with present imperilment across the amphibian tree of life. Nat. Ecol. Evol. 2(5), 850–858.

Jorgensen, M.E., Reilly, S.M., 2013. Phylogenetic patterns of skeletal morphometrics and pelvic traits in relation to locomotor mode in frogs. J. Evol. Biol. 26(5), 929–943.

Kalyaanamoorthy, S., Minh, B.Q., Wong, T.K., Von Haeseler, A., Jermiin, L.S., 2017. ModelFinder: fast model selection for accurate phylogenetic estimates. Nat. Methods 14(6), 587–589.

Katoh, K., Standley, D.M., 2013. MAFFT Multiple sequence alignment software Version 7: Improvements in performance and usability. Mol. Biol. Evol. 30, 772–780.

Kjer, K.M., Honeycutt, R.L., 2007. Site specific rates of mitochondrial genomes and the phylogeny of eutheria. BMC Evol. Biol. 7(1), 1–9.

Kok, P.J.R., 2005. A new genus and species of gymnophthalmid lizard (Squamata: Gymnophthalmidae) from Kaieteur National Park, Guyana. Bull. Inst. r. sci. nat. Belg. Biol. 75, 35–45

Kok, P.J.R., 2009. Lizard in the clouds: a new highland genus and species of Gymnophthalmidae (Reptilia: Squamata) from Maringma tepui, western Guyana. Zootaxa 1992, 53–67.

Kok, P.J.R., 2013. Islands in the Sky: Species Diversity, Evolutionary History, and Patterns of Endemism of the Pantepui Herpetofauna. PhD thesis, Leiden University, the Netherlands.

Kok, P.J.R., 2015. A new species of the Pantepui endemic genus *Riolama* (Squamata: Gymnophthalmidae) from the summit of Murisipán-tepui, with the erection of a new gymnophthalmid subfamily. Zool. J. Linn. Soc. 174(3), 500–518.

Kok, P.J.R., 2023a. Bones and all: A new critically endangered Pantepui species of *Stefania* (Anura: Hemiphractidae) and a new osteological synapomorphy for the genus. Zool. Lett. 9(11), 1–20.

Kok, P.J.R., 2023b. Out of sight, but not out of mind: A name for the *Stefania* (Anura: Hemiphractidae) from the summit of Murisipán-tepui (Bolívar State, Venezuela). J. Vertebr. Biol. 72 (23024), 1–17.

Kok, P.J.R., Laking, A., Smith, C., Berti, A., Martel, A., Pasmans, F., 2022. Tourism may threaten wildlife disease refugia. Conserv. Lett. 15, e12902.

Kok, P.J.R., MacCulloch, R.D., Means, D.B., Roelants, K., Van Bocxlaer, I., Bossuyt, F., 2012. Low genetic diversity in tepui summit vertebrates. Curr. Biol. 22, R589–R590.

Kok, P.J.R., Means, D.B., 2023. Hiding in the mists: Molecular phylogenetic position and description of a new genus and species of snake (Dipsadidae: Xenodontinae) from the remote cloud forest of the Lost World. Zool. J. Linn. Soc. 10.1093/zoolinnean/zlad082

Kok, P.J.R., Ratz, S., Tegelaar, M., Aubret, F., Means, D.B., 2015. Out of taxonomic limbo: a name for the species of *Tepuihyla* (Anura: Hylidae) from the Chimanta Massif, Pantepui region, northern South America. Salamandra 51, 283–314.

Kok, P.J.R., Ratz, S., MacCulloch, R.D., Lathrop, A., Dezfoulian, R., Aubret, F., Means, D.B., 2018. Historical biogeography of the palaeoendemic toad genus *Oreophrynella* (Amphibia: Bufonidae) sheds a new light on the origin of the Pantepui endemic terrestrial biota. J. Biogeogr. 45(1), 26–36.

Kok, P.J.R., Russo, V.G., Ratz, S., Means, D.B., MacCulloch, R.D., Lathrop, A., Aubret, F., Bossuyt, F., 2017. Evolution in the South American 'Lost World': insights

from multilocus phylogeography of stefanias (Anura, Hemiphractidae, *Stefania*). J. Biogeogr. 44, 170–181.

Kok, P.J.R., van Doorn, L., Dezfoulian, R., 2019. Predation by non-bioluminescent firefly larvae on a tepui-summit endemic toad. Cur. Biol. 29(22), R1170–R1171.

Leite, Y.L., Kok, P.J.R., Weksler, M., 2015. Evolutionary affinities of the 'Lost World'mouse suggest a late Pliocene connection between the Guiana and Brazilian shields. J. Biogeogr. 42(4), 706–715.

Linck, E.B., Freeman, B.G., Cadena, C.D., Ghalambor, C.K., 2021. Evolutionary conservatism will limit responses to climate change in the tropics. Biol. Lett. 17(10), 20210363.

Linnaeus, C., 1758. *Systema Naturae per Regna Tria Naturae, Secundum Classes, Ordines, Genera, Species, cum Characteribus, Differentiis, Synonymis, Locis*. 10th Edition. Volume 1. Stockholm, Sweden: L. Salvii.

Lister, B.C., Garcia, A., 2018. Climate-driven declines in arthropod abundance restructure a rainforest food web. Proc. Natl. Acad. Sci. U.S.A. 115(44), E10397–E10406.

Lösel, P.D., van de Kamp, T., Jayme, A., Ershov, A., Faragó, T., Pichler, O., Jerome, N.T., Aadepu, N., Bremer, S., Suren A., Chilingaryan, S.A, Heethoff, M., Kopmann, A., Odar, O., Schmelzle, S., Zuber, M., Wittbrodt, J., Baumbach, T., Heuveline, V., 2020. Introducing Biomedisa as an open-source online platform for biomedical image segmentation. Nat. Comm. 11(1), 1–14.

Lynch, J.D. 1973. The transition from archaic to advanced frogs. *in* Evolutionary biology of the anurans: contemporary research on major problems, Vial J.L. (Ed.), pp. 133–182. University of Missouri Press, Columbia.

Lynch, J.D., Duellman, W.E., 1997. Frogs of the genus *Eleutherodactylus* in western Ecuador. University of Kansas Special Publication, 23, 1–236.

MacCulloch, R.D., Lathrop, A., 2002. Exceptional diversity of *Stefania* (Anura: Hylidae) on Mount Ayanganna, Guyana: three new species and new distribution records. Herpetologica 58(3), 327–346.

MacCulloch, R.D., Lathrop, A., 2005. Hylid frogs from Mount Ayanganna, Guyana: new species, redescriptions, and distributional records. Phyllomedusa 4(1), 17–37.

MacCulloch, R.D., Lathrop, A., Kok, P.J.R., Minter, L.R., Khan, S.Z., Barrio-Amoros, C.L., 2008. A new species of *Adelophryne* (Anura: Eleutherodactylidae) from Guyana, with additional data on *A. gutturosa*. Zootaxa 1884(1), 36–50.

Manes, S., Costello, M.J., Beckett, H., Debnath, A., Devenish-Nelson, E., Grey, K.A., Jenkins, R., Khan, T.M., Kiessling, W., Krause, C., Maharaj, S.S., 2021. Endemism increases species' climate change risk in areas of global biodiversity importance. Biol. Cons. 257, 109070.

McDiarmid, R.W., Donnelly, M.A., 2005. The herpetofauna of the Guayana Highlands: amphibians and reptiles of the Lost World. *in* Ecology and evolution in the tropics: a

herpetological perspective, Donnelly, M.A., Crother, B.I., Guyer, C., Wake, M.H., White, M.E. (Eds.), pp. 461–560. University of Chicago Press.

Mendoza, Á.M., Ospina, O.E., Cárdenas-Henao, H., García-R, J.C., 2015. A likelihood inference of historical biogeography in the world's most diverse terrestrial vertebrate genus: Diversification of direct-developing frogs (Craugastoridae: *Pristimantis*) across the Neotropics. Mol. Phyl. Evol. 85, 50–58.

Moraes, L.J., Werneck, F.P., Réjaud, A., Rodrigues, M.T., Prates, I., Glaw, F., Kok, P.J.R., Ron, S.R., Chaparro, J.C., Osorno-Muñoz, M., Dal Vechio, F., Recoder, R.S., Marques-Souza, S., Rojas, R.R., Demay, L., Hrbek, T., Fouquet, A., 2022. Diversification of tiny toads (Bufonidae: *Amazophrynella*) sheds light on ancient landscape dynamism in Amazonia. Biol. J. Linn. Soc. 136(1), 75–91.

Motta, A.P., Taucce, P.P.G., Haddad, C.F.B., Canedo, C., 2021. A new terraranan genus from the Brazilian Atlantic Forest with comments on the systematics of Brachycephaloidea (Amphibia: Anura). J. Zoolog. Syst. Evol. 59(3), 663–679.

Myers, C.W., Donnelly, M.A., 2001. Herpetofauna of the Yutajé-Corocoro Massif, Venezuela: second report from the Robert G. Goelet American Museum - Terramar Expedition to the Northwestern Tepuis. Bull. Amer. Mus. Nat. Hist. (261), 1–85.

Myers, C.W., Williams, E.E., McDiarmid, R.W., 1993. A new anoline lizard (*Phenacosaurus*) from the highland of Cerro de la Neblina, southern Venezuela. Am. Mus. Novit. 3070, 1–15.

Ogden, T.H., Rosenberg, M.S., 2007. How should gaps be treated in parsimony? A comparison of approaches using simulation. Mol. Phyl. Evol. 42(3), 817–826.

Ortiz, D.A., Hoskin, C.J., Werneck, F.P., Réjaud, A., Manzi, S., Ron, S.R., Fouquet, A., 2022. Historical biogeography highlights the role of Miocene landscape changes on the diversification of a clade of Amazonian tree frogs. Org. Divers. Evol. in press.

Ospina-Sarria, J.J., Grant, T., 2021. New phenotypic synapomorphies delimit three molecular-based clades of New World direct-developing frogs (Amphibia: Anura: Brachycephaloidea). Zool. J. Linn. Soc. 195, 976–994.

Padial, J.M., Grant, T., Frost, D.R., 2014. Molecular systematics of terraranas (Anura: Brachycephaloidea) with an assessment of the effects of alignment and optimality criteria. Zootaxa 3825(1), 1–132.

Páez-Moscoso, D.J., Guayasamin, J.M., 2012. Species limits in the Andean toad genus *Osornophryne* (Bufonidae). Mol. Phyl. Evol. 65(3), 805–822.

Páez, N.B., Ron, S.R., 2019. Systematics of *Huicundomantis*, a new subgenus of *Pristimantis* (Anura, Strabomantidae) with extraordinary cryptic diversity and eleven new species. ZooKeys 868, 1.

Pellegrino, K.C.M., Brunes, T.O., Souza, S.M., Laguna, M.M., Avila-Pires, T.C.S., Hoogmoed, M.S., Rodrigues, M.T., 2018. On the distinctiveness of *Amapasaurus*, its relationship with *Loxopholis* Cope 1869, and description of a new genus for *L.*

guianensis and *L. hoogmoedi* (Gymnophthalmoidea/Ecpleopodini: Squamata). Zootaxa 4441(2), 332–346.

Pinheiro, P.D., Kok, P.J.R., Noonan, B.P., Means, D.B., Haddad, C.F., Faivovich, J., 2019. A new genus of Cophomantini, with comments on the taxonomic status of *Boana liliae* (Anura: Hylidae). Zool. J. Linn. Soc. 185(1), 226–245.

Platts, P.J., Mason, S.C., Palmer, G., Hill, J.K., Oliver, T.H., Powney, G.D., Fox, R., Thomas, C.D., 2019. Habitat availability explains variation in climate-driven range shifts across multiple taxonomic groups. Sci. Rep. 9(1), 1–10.

Pyron, R.A., Wiens, J.J., 2011. A large-scale phylogeny of Amphibia including over 2800 species, and a revised classification of extant frogs, salamanders, and caecilians. Mol. Phyl. Evol. 61(2), 543–583.

Rahbek, C., Borregaard, M.K., Colwell, R.K., Dalsgaard, B.O., Holt, B.G., Morueta-Holme, N., Nogues-Bravo, D., Whittaker, R.J., Fjeldså, J., 2019. Humboldt's enigma: What causes global patterns of mountain biodiversity?. Science 365(6458), 1108–1113.

Rangel, T.F., Edwards, N.R., Holden, P.B., Diniz-Filho, J.A.F., Gosling, W.D., Coelho, M.T.P., Cassemiro, F.A., Rahbek, C., Colwell, R.K., 2018. Modeling the ecology and evolution of biodiversity: Biogeographical cradles, museums, and graves. Science 361(6399), p.eaar5452.

Recoder, R., Prates, I., Marques-Souza, S., Camacho, A., Nunes, P.M.S., Dal Vechio, F., Ghellere, J. M., McDiarmid, R.W., Rodrigues, M.T., 2020. Lizards from the Lost World: two new species and evolutionary relationships of the Pantepui highland *Riolama* (Gymnophthalmidae). Zool. J. Linn. Soc. 190(1), 271–297.

Reilly, S., Jorgensen, M., 2011. The evolution of jumping in frogs: morphological evidence for the basal anuran locomotor condition and the radiation of locomotor systems in crown group anurans. J. Morphol. 272, 149–168.

Rolland, J., Condamine, F.L., 2019. The contribution of temperature and continental fragmentation to amphibian diversification. J. Biogeogr. 46(8), 1857–1873.

Roure, B., Baurain, D., Philippe, H., 2013. Impact of missing data on phylogenies inferred from empirical phylogenomic data sets. Mol. Biol. Evol. 30(1), 197–214.

Rull, V., 2004. Biogeography of the 'Lost World': a palaeoecological perspective. Earth Sci. Rev. 67(1–2), 125–137.

Rull, V., Vegas-Vilarrúbia, T., 2020. The Pantepui "Lost World": towards a biogeographical, ecological and evolutionary synthesis of a pristine Neotropical sky-island archipelago. in Rull, V., Carnaval, A.C.Q (Eds.), Neotropical Diversification: Patterns and Processes, pp. 369–413.

Sanderson, M.J., Shaffer, H.B., 2002. Troubleshooting molecular phylogenetic analyses. Annu. Rev. Ecol. Evol. Syst. 33(1), 49–72.

Santos, J.C., Coloma, L.A., Summers, K., Caldwell, J.P., Ree, R., Cannatella, D.C., 2009. Amazonian amphibian diversity is primarily derived from later Miocene Andean lineages. PLoS Biol. 7, 448–461.

Smale, D.A., Wernberg, T., Oliver, E.C., Thomsen, M., Harvey, B.P., Straub, S.C., Burrows, M.T., Alexander, L.V., Benthuysen, J.A., Donat, M.G., Feng, M., 2019. Marine heatwaves threaten global biodiversity and the provision of ecosystem services. Nat. Clim. Change 9(4), 306–312.

Smith, B.T., Mauck III, W.M., Benz, B.W., Andersen, M.J. ,2020. Uneven missing data skew phylogenomic relationships within the lories and lorikeets. Genome Biol. Evol. 12(7), 1131–1147.

Streicher, J.W., Miller, E.C., Guerrero, P.C., Correa, C., Ortiz, J.C., Crawford, A.J., Pie, M.R. and Wiens, J.J., 2018. Evaluating methods for phylogenomic analyses, and a new phylogeny for a major frog clade (Hyloidea) based on 2214 loci. Mol. Phyl. Evol. 119, 128–143.

Taucce, P.P., Canedo, C., Parreiras, J.S., Drummond, L.O., Nogueira-Costa, P., Haddad, C.F., 2018. Molecular phylogeny of *Ischnocnema* (Anura: Brachycephalidae) with the redefinition of its series and the description of two new species. Mol. Phyl. Evol. 128, 123–146.

Trisos, C.H., Merow, C., Pigot, A.L., 2020. The projected timing of abrupt ecological disruption from climate change. Nature, 580(7804), 496–501.

Trueb, L., 1973. Bones, frogs, and evolution. In: Vial JL, editor. Evolutionary Biology of the Anurans: Contemporary Research on Major Problems. University of Missouri Press. 65–132.

Vacher, J.-P., Kok, P.J.R., Rodrigues, M.T., Lima, A.P., Hrbek, T., Werneck, F.P., Manzi, S., Thébaud, C., Fouquet, A., 2023. Diversification of terrestrial frogs within the Guiana Shield: from highlands to lowlands and successive loss and reacquisition of endotrophy in *Anomaloglossus* (Aromobatidae). Mol. Phyl. Evol. in press.

Vences, M., Guayasamin, J.M., Miralles, A., De La Riva, I., 2013. To name or not to name: criteria to promote economy of change in supraspecific Linnean classification schemes. Zootaxa 3636(2), 201–244.

Wiens, J.J., Camacho, A., Goldberg, A., Jezkova, T., Kaplan, M.E., Lambert, S.M., Miller, E.C., Streicher, J.W., Walls, R.L., 2019. Climate change, extinction, and Sky Island biogeography in a montane lizard. Mol. Ecol. 28(10), 2610–2624.

Yang, Z., 2006. Computational Molecular Evolution. Oxford University Press, New York.

Zweifel, R.G., 1986. A new genus and species of microhylid frog from the Cerro de la Neblina region of Venezuela and a discussion of relationships among New World microhylid genera. Am. Mus. Novit. 2863, 1–24.

Fig. 1. Topographic maps of (A) northern South America; (B) southwestern part of Pantepui; (C) Pico da Neblina Massif, the study area; and (D, E) pictures of the habitat where the two new species have been found.

Fig. 2. Time-calibrated phylogenetic reconstructions from Bayesian analysis (BEAST) using mitogenomes and nuDNA loci combined (results for nuDNA loci and mitogenomes separately are provided in Fig. S3). Nodes without numbers have pp = 1; orange dots correspond to time calibration without monophyly constraints; red dots indicate time calibration and monophyly constraints.

Fig. 3. The holotype of *Neblinaphryne mayeri* gen. nov. sp. nov. (MZUSP A159564). (A) dorsal view, (B) ventral view, (C) left side of head, (D) right palm, (E) right sole, all from the preserved animal. (F) illustrates a female paratype (MZUSP A159578) in vivo.

Fig. 4. Three-dimensional model of the cranium of a female paratype of *Neblinaphryne mayeri* gen. nov. sp. nov. (MZUSP A159552) based on µCT imagery. Top left. Dorsal view. Top right. Ventral view. Middle. Frontal view. Bottom. Right lateral view. Abbreviations: ang = angulosplenial, ang.cp = coronoid process of the angulosplenial, col = columella, c.p = cultriform process, d = dentary, exo = exoccipital, fp = frontoparietal, lam.p = lamina perpendicularis, mmk = mentomeckelian, mx = maxilla, na = nasal, na.mp = maxillary process of the nasal, neo = neopalatine, p.f = pars facialis, pmx = premaxilla, pmx.ap = alary process of the premaxilla, pmx.lp = lateral process of the premaxilla, pmx.pp = palatine process of the premaxilla, pro = prootic, psp = parasphenoid, psp.ap = alary process of the parasphenoid, psp.pp = posteromedial process of the parasphenoid, pt = pterygoid, pt.ar = anterior ramus of the pterygoid, pt.pr = posterior ramus of the pterygoid, qua = quadratojugal, sph = sphenethmoid, squa = squamosal, squa.or = otic ramus of the squamosal, squa.vr = ventral ramus of the squamosal, v = vomer. Red circles depict the potential presence of a vestigial left septomaxilla (vs. absence on the right side).

Fig. 5. Three-dimensional model of the complete skeleton of a female paratype of *Neblinaphryne mayeri* gen. nov. sp. nov. (MZUSP A159552), based on µCT imagery. Top left: Dorsal view. Top right: Ventral view. Middle: Frontal view. Bottom: Right lateral view.

Fig. 6. The holotype of *Caligophryne doylei* gen. nov. sp. nov. (MZUSP A159537). (A) dorsal view, (B) ventral view, (C) left side of head, (D) right palm, (E) left sole, all from the preserved specimen. (F) the holotype in life.

Fig. 7. Three-dimensional model of the cranium of a female paratype of *Caligophryne doylei* gen. nov. sp. nov. (MZUSP A159536), based on µCT imagery. Top left. Dorsal view. Top right. Ventral view. Middle. Frontal view. Bottom. Right lateral view. Abbreviations: ang =

angulosplenial, ang.cp = coronoid process of the angulosplenial, col = columella, c.p = cultriform process, d = dentary, exo = exoccipital, fp = frontoparietal, lam.p = lamina perpendicularis, mmk = mentomeckelian, mx = maxilla, na = nasal, na.mp = maxillary process of the nasal, neo = neopalatine, p.f = pars facialis, pmx = premaxilla, pmx.ap = alary process of the premaxilla, pmx.lp = lateral process of the premaxilla, pmx.pp = palatine process of the premaxilla, pro = prootic, psp = parasphenoid, psp.ap = alary process of the parasphenoid, psp.pp = posteromedial process of the parasphenoid, pt = pterygoid, pt.ar = anterior ramus of the pterygoid, pt.mr = medial ramus of the pterygoid, pt.pr = posterior ramus of the pterygoid, qua = quadratojugal, smx = septomaxilla, sph = sphenethmoid, squa = squamosal, squa.or = otic ramus of the squamosal, squa.vr = ventral ramus of the squamosal, squa.zr = zygomatic ramus of the squamosal, v = vomer.

Fig. 8. Three-dimensional model of the complete skeleton of a female paratype of *Caligophryne doylei* gen. nov. sp. nov. (MZUSP A159536), based on µCT imagery. Top left: Dorsal view. Top right: Ventral view. Middle: Frontal view. Bottom: Right lateral view.

Table 1. Morphometric variation (mean + standard deviation, min–max of females and males) of *Caligophryne doylei* gen. nov. sp. nov. and *Neblinaphryne mayeri* gen. nov. sp. nov. Raw measurements of each specimen are available at: to be added upon ms acceptance.

	Caligophryne doylei gen. nov. sp. nov.		*Neblinaphryne mayeri* gen. nov. sp. nov.	
Sex	Females n=10	Males n=10	Females n=17	Males n=15
SVL	28.7 ± 4.1 (18.8–33.8)	24.0 ± 4.3 (19.7–33.1)	18.1 ± 0.9 (15.9–20.1)	16.7 ± 1.9 (14.0–19.2)
HL	12.3 ± 1.4 (8.9–14.1)	10.4 ± 1.7 (8.6–14.0)	6.6 ± 0.6 (5.7–7.5)	6.2 ± 0.9 (4.9–7.7)
HW	13.1 ± 1.5 (9.3–14.7)	10.6 ± 2.0 (8.4–14.6)	6.4 ± 0.5 (5.5–7.3)	6.0 ± 0.8 (4.9–7.2)
IND	3.0 ± 0.3 (2.2–3.3)	2.6 ± 0.4 (2.2–3.2)	2.1 ± 0.1 (1.9–2.4)	1.9 ± 0.2 (1.5–2.3)

Journal Pre-proofs

END	3.3 ± 0.4 (2.5–3.9)	2.7 ± 0.4 (2.3–3.6)	1.3 ± 0.1 (1.1–1.4)	1.1 ± 0.2 (0.7–1.3)
ED	3.2 ± 0.3 (2.7–3.6)	2.9 ± 0.4 (2.1–3.4)	2.2 ± 0.2 (2.0–2.5)	2.1 ± 0.2 (1.9–2.5)
IOD	3.3 ± 0.4 (2.8–3.9)	2.6 ± 0.3 (2.1–3.3)	2.1 ± 0.2 (1.7–2.3)	1.7 ± 0.2 (1.2–2.1)
UEW	2.2 ± 0.2 (1.8–2.5)	1.9 ± 0.2 (1.4–2.2)	1.4 ± 0.1 (1.2–1.5)	1.3 ± 0.1 (1.2–1.5)
TD	1.6 ± 0.2 (1.4–1.8)	1.5 ± 0.3 (1.2–1.8)	-	-
ARM	6.7 ± 0.8 (5.1–7.7)	5.5 ± 0.9 (4.6–7.3)	4.5 ± 0.2 (4.1–5.0)	4.2 ± 0.4 (3.3–4.8)
HAN	8.1 ± 1.3 (5.5–10.0)	6.3 ± 1.5 (4.8–9.7)	4.0 ± 0.2 (3.7–4.3)	3.8 ± 0.5 (2.9–4.5)
TH	14.7 ± 1.7 (10.3–16.5)	11.5 ± 2.1 (8.4–15.5)	8.2 ± 0.3 (7.6–8.8)	7.5 ± 0.8 (6.0–9.0)
TL	13.8 ± 1.5 (10.0–15.2)	11.3 ± 1.8 (9.3–14.8)	7.6 ± 0.3 (7.0–8.1)	7.1 ± 0.7 (5.6–8.0)
TAL	8.4 ± 1.0 (6.3–9.9)	7.0 ± 1.2 (5.7–9.3)	5.6 ± 0.3 (5.1–6.0)	5.3 ± 0.5 (4.1–6.1)
FTL	14.4 ± 2.0 (10.0–16.9)	11.4 ± 2.2 (9.0–16.0)	8.2 ± 0.4 (7.5–9.2)	7.9 ± 0.7 (6.7–9.0)

Journal Pre-proofs